

# A Survey of Merger Remnants II: The Emerging Kinematic and Photometric Correlations <sup>1</sup>

B. Rothberg

*Space Telescope Science Institute, 3700 San Martin Drive Baltimore, MD 21218*

rothberg@stsci.edu

R. D. Joseph

*Institute for Astronomy, 2680 Woodlawn Drive, Honolulu, HI 96822*

## ABSTRACT

This paper is the second in a series exploring the properties of 51 *optically* selected, single-nuclei merger remnants. Spectroscopic data have been obtained for a sub-sample of 38 mergers and combined with previously obtained infrared photometry to test whether mergers exhibit the same correlations as elliptical galaxies among parameters such as stellar luminosity and distribution, central stellar velocity dispersion ( $\sigma_o$ ), and metallicity. Paramount to the study is to test whether mergers lie on the Fundamental Plane. Measurements of  $\sigma_o$  have been made using the Ca triplet absorption line at 8500 Å for all 38 mergers in the sub-sample. Additional measurements of  $\sigma_o$  were made for two of the mergers in the sub-sample using the CO absorption line at 2.29  $\mu\text{m}$ . The results indicate that mergers show a strong correlation among the parameters of the Fundamental Plane but fail to show a strong correlation between  $\sigma_o$  and metallicity ( $\text{Mg}_2$ ). In contrast to earlier studies, the  $\sigma_o$  of the mergers are consistent with objects which lie somewhere between intermediate-mass and luminous giant elliptical galaxies. However, the discrepancies with earlier studies appears to correlate with whether the Ca triplet or CO absorption lines are used to derive  $\sigma_o$ , with the latter almost always producing smaller values. Finally, the photometric and kinematic data are used to demonstrate for the first time that the central phase-space density of mergers are equivalent to elliptical galaxies. This resolves a long-standing criticism of the merger hypothesis.

*Subject headings:* galaxies: evolution—galaxies: formation—galaxies: interactions—galaxies: peculiar —galaxies: kinematics and dynamics—galaxies: structure

---

<sup>1</sup>Some of the data presented herein were obtained at the W.M. Keck Observatory, which is operated as a scientific partnership among the California Institute of Technology, the University of California and the National Aeronautics and Space Administration. The Observatory was made possible by the generous financial support of the W.M. Keck Foundation.

## 1. Introduction

This paper is the second in a series addressing the viability of the Toomre Merger Hypothesis (Toomre 1977) that two merging spiral galaxies can produce a bona fide elliptical galaxy. The first paper (Rothberg & Joseph 2004), hereafter Paper I, used  $K$ -band infrared photometry to determine whether mergers undergo violent relaxation, as predicted by numerical models, how their structural parameters compare with elliptical galaxies, and investigate whether mergers have luminosities consistent with  $L^*$  ellipticals. Fifty-one advanced merger remnants were *optically* selected for the study. The results showed that stellar light profile of most of the mergers could be modeled fairly well with a de Vaucouleurs  $r^{1/4}$  profile. This profile shape is produced as a result of the dissipationless collapse of a stellar system during formation (van Albada 1982). One way to initiate this is the process of violent relaxation (Lynden-Bell 1967; Hjorth & Madsen 1991), in which the stars are scattered by the net gravitational field of the system. Numerical models by Barnes (1988, 1992), among others have shown that mergers undergo violent relaxation, and the net result produces a change in the stellar distribution from an exponential light profile, to one in which light approximately follows an  $r^{1/4}$  profile (the same profile shape observed in elliptical galaxies). The results also showed that the mergers are fairly luminous at  $K$ -band, nearly two-thirds have  $L \geq 1 L^*_{ellip}$ , and the  $K$ -band isophotal shapes of the mergers appear to be predominantly disk.

However, photometry alone is insufficient to conclude whether mergers can produce real elliptical galaxies. While an  $r^{1/4}$  profile is consistent with the merger hypothesis, information about the stellar dynamics of the system provides a stronger test. Observations have shown that spiral bulges, S0 and elliptical galaxies all share a common correlation between certain kinematic and photometric parameters. In particular, these objects are known to lie along a two-dimensional plane, or “Fundamental Plane,” embedded in a three-dimensional space comprised of the central velocity dispersion ( $\sigma_o$ ), half-light or “effective”-radius ( $r_{\text{eff}}$ ) and the surface brightness within the effective radius ( $\langle \mu \rangle_{\text{eff}}$ ) (Djorgovski & Davis 1987; Bender, Burstein, & Faber 1992). While the small scatter in the Fundamental Plane makes it useful as a distance indicator, the tight correlation among the observed parameters provides important clues about the underlying physics of these systems. A similar relationship to the Fundamental Plane can be derived using the Virial Theorem, assuming that  $M/L \propto L^\alpha$  is constant, and that elliptical galaxies and bulges form a homologous family in their scaling relations. This suggests that the empirically derived Fundamental Plane is a representation of the Virial Theorem. If mergers lie on or near the Fundamental Plane, this suggests that they are physically similar to elliptical galaxies.

Elliptical galaxies also show a strong correlation between  $\sigma_o$  and  $\text{Mg}_2$ , which serve as a proxy for mass and metallicity (Tonry & Davis 1981; Terlevich et al. 1981). The deeper the potential well, the more the stellar populations are metal enriched. The kinematic data presented here allow this relationship to be tested for the first time among mergers. It has been shown that mergers undergo strong star-formation, (Schweizer 1987; Joseph & Wright 1985) likely triggered by the dissipation of gas from the progenitor galaxies. A test of the mass-metallicity relation may provide constraints on the stellar populations present, or forming in mergers and how they compare with those in elliptical galaxies.

The kinematic data presents a unique opportunity to directly address an early, but serious criticism of the mergers-make-ellipticals hypothesis; that the stellar phase-space densities of elliptical and spiral galaxies are very different. Carlberg (1986) used surface photometry of galaxy cores in conjunction with velocity dispersions to compare the phase-space densities of elliptical and spiral galaxies. The results showed that all but the brightest ellipticals have significantly higher phase-space densities than spirals. According to the collisionless Boltzmann equation, the phase-space density of a stellar system remains constant or decreases. It cannot increase. Therefore, most elliptical galaxies cannot form from purely dissipationless (stellar-only) mergers. This led Gunn (1987) to comment, “I do not think you can make rocks by merging clouds.” Hernquist, Spergel, & Heyl (1993) explored the evolution of phase-space densities in mergers using numerical simulations. The results were consistent with Carlberg’s findings. Stellar disks lack sufficient material at high-phase space densities to form elliptical galaxies. One way to overcome this is via a starburst induced by dissipative collapse of the gas. Barnes & Hernquist (1991), among others, used hydrodynamical simulations to show that tidal forces in a merger can drive a significant fraction of the gas into the central region. The gas is not subject to the collisionless Boltzmann equation and becomes more centrally concentrated than the stars. The infall can fuel a starburst, producing more stars and increasing the phase-space density of the merger. Mihos & Hernquist (1994) included the effects of dissipative collapse in their numerical simulations of mergers. Their models predict that when the gas falls to the center of the merger, a strong starburst is triggered. The resulting central starburst should affect the shape of the surface brightness profile, producing a sharp increase in luminosity near the nucleus. The results from Paper I showed that nearly one-third of the mergers show evidence of just such an increase in luminosity near the nucleus, producing surface brightness profiles that rise significantly above an  $r^{1/4}$  profile. The kinematic data presented here make it possible for the first time to directly measure the phase-space density of mergers and compare them with spiral and elliptical galaxies.

To date, few kinematic studies of mergers have been undertaken. The largest, and most in-depth kinematic study was conducted by Lake & Dressler (1986). They measured the  $\sigma_0$  of 13 mergers from the Atlas of Peculiar Galaxies (Arp 1966) and A Catalogue of Southern Peculiar Galaxies (Arp & Madore 1987) using both the Mg *Ib* ( $\lambda \sim 5170 \text{ \AA}$ ) and Ca triplet ( $\lambda \sim 8500 \text{ \AA}$ ) stellar absorption lines. The central velocity dispersions were then plotted against  $M_B$  to test whether they fit the Faber-Jackson relation (Faber & Jackson 1976). This relation is a correlation between the total luminosity,  $L$ , and  $\sigma_0$ , such that  $L \propto \sigma^4$ . It is similar to the Fundamental Plane, but the relation produces a larger scatter, implying the presence of second parameter. Lake & Dressler predicted that the mergers should be 1.5 mag brighter, with  $\sigma_0 \sim 30\%$  smaller than elliptical galaxies. The results showed that the mergers were only  $\sim 0.4$  mag brighter in luminosity for a given  $\sigma_0$ . The differences between the mergers and ellipticals in the Coma and Virgo clusters were not outside the range of differences seen between other samples of elliptical galaxies. They also found that the Mg *Ib* absorption lines were more problematic than the Ca triplet lines for deriving  $\sigma_0$ . Contamination from nearby emission lines, most likely caused by star-formation and/or young stars, can interfere with the Mg *Ib* lines. Lake & Dressler suggested that using the *H*-band to mea-

sure the luminosity and the Ca triplet lines to derive  $\sigma_0$  would be more effective because they are less likely to be affected by star-formation, and are more sensitive to the older stellar population.

No further studies of mergers using the Ca triplet absorption line to derive velocity dispersions have been made, and no studies have ever been conducted using the Ca triplet line and the Fundamental Plane. Later studies have substituted the use of the Ca triplet line with the CO absorption line at  $2.29 \mu\text{m}$  (and sometimes at  $1.63 \mu\text{m}$ ) to study whether mergers lie on or near the Fundamental Plane (see Gaffney, Lester, & Doppmann (1995) for a discussion of the use of the  $2.29 \mu\text{m}$  CO absorption line for kinematic studies). The switch to the CO line was motivated by studies of Luminous and Ultra-Luminous Infrared Galaxies. LIRGs and ULIRGs are objects with  $L_{FIR} \geq 10^{11} L_\odot$  and  $10^{12} L_\odot$  respectively, where  $L_{FIR}$  is measured from 8-1000  $\mu\text{m}$  (see Sanders & Mirabel (1996) for a more in-depth look). A vast majority of these objects have disturbed morphologies consistent with an ongoing merger. The CO line was chosen primarily to avoid the effects of high optical extinction caused by dust in LIRG/ULIRGs.

Several LIRG/ULIRG merger studies been made using the  $2.29 \mu\text{m}$  CO absorption line to obtain velocity dispersions, including Doyon et al. (1994), Shier & Fischer (1998), and James et al. (1999). Oliva et al. (1995) and Genzel et al. (2001) used both the  $2.29 \mu\text{m}$  and  $1.63 \mu\text{m}$  CO absorption line. However, a major difference between these studies and the one presented here lies in the sample selection. The mergers presented in this paper have been selected based on *optical* morphology alone, and not based on their infrared luminosity. In addition, all of the mergers in this paper have only one nucleus, in contrast to earlier LIRG/ULIRG kinematic studies, which included objects with two nuclei. Of the 38 mergers in this sample for which velocity dispersions have been obtained, only 8 have been previously measured using the Ca triplet, and 8 have been previously measured using the infrared CO absorption feature. One object, NGC 7252, has been studied before using both the Ca triplet and CO studies, mainly because it is considered a “canonical” merger.

$K$ -band photometry was selected for the survey for two reasons. First, dust extinction is  $\sim 1/10^{th}$  that at  $V$ -band. Second, the blackbody emission of older, late-type stars, which trace the majority of the stellar mass in both elliptical and spiral galaxies, peaks in the near-infrared beyond  $1 \mu\text{m}$  (Aaronson 1981).

However, one problem with using the  $K$ -band is the possibility of contamination from Asymptotic Giant Branch (AGB) stars. These stars also peak in luminosity in the near-infrared. Mouhcine & Lançon (2002) modeled the contribution of AGB stars to the total  $K$ -band luminosity for a single-burst population. They found that the contribution evolves rapidly from a few percent at  $\simeq 0.1$  Gyr to  $\simeq 60\%$  of the light at 0.6-0.7 Gyr and then quickly declines soon after to  $\leq 30\%$ . The contribution to the integrated light is also directly proportional to metallicity. Yet, the contribution from AGB stars to the total  $K$ -band light is still less than the contribution of young stars to the integrated light at optical wavelengths.

The Ca triplet lines at 8498.0, 8542.1, and 8662.1  $\text{\AA}$  were selected as the primary tool to measure the stellar velocity dispersions because they are strong, well-separated, and narrow (Dressler 1984). These lines are particularly strong in late-type giants. Other optical lines are often broader,

too complex, or very sensitive to template mismatch. Absorption lines at shorter wavelengths are also more likely to be contaminated by strong nearby emission lines from in galaxies undergoing star-formation or with young stellar populations. Finally, the more red-ward Ca triplet lines are somewhat less affected by extinction than absorption lines at shorter wavelengths.

Velocity dispersions have also been measured using the CO absorption feature at  $2.29 \mu\text{m}$  for two galaxies in the sample, NGC 1614 and NGC 2623. These mergers are both classified as LIRGs. As noted earlier, the selection of the CO stellar absorption line is primarily motivated by the desire to avoid as much extinction as possible because LIRG/ULIRGs are known to be quite dusty. The CO line at  $2.29 \mu\text{m}$  is quite strong and well-defined. However, there is one serious drawback. The CO absorption line is sensitive not only to late-type giant stars, but the presence of red supergiants and strong starbursts. Velocity dispersions derived from this line may not be probing the same late-type stars as other stellar absorption lines. Furthermore, the presence of hot-dust from a starburst, or the presence of an AGN can “fill-in” the CO line and affect the derived velocity dispersions. There is already some evidence to suggest that velocity dispersions measured from the CO absorption line do not match those measured from lines at shorter wavelengths Silge & Gebhardt (2003) found that, for a sample of 25 early-type galaxies, velocity dispersions obtained from CO were generally smaller, sometimes by as much as 40%. A similar result was found for the mergers and will be discussed subsequently.

An important part of comparing the photometric and kinematic properties of mergers with those of elliptical galaxies rests on assuring that the comparison is made using the same type of diagnostic tools. Until recently, a comprehensive infrared study of elliptical galaxies did not exist. The first large survey was done by Mobasher et al. (1999) in which they constructed a  $K$ -band fundamental plane for 48 early-type galaxies in Coma. Pahre (1999) (hereafter P99), conducted a  $K$ -band photometric study of 251 early-type galaxies from several clusters, groups, and in the field. Using this data along with velocity dispersions and  $\text{Mg}_2$  measurements obtained from the literature, Pahre, Djorgovski, & de Carvalho (1998) (hereafter P98) conducted an in-depth analysis of several elliptical galaxy correlations, including the Fundamental Plane. The  $K$ -band was selected for these studies primarily for the same reasons as the merger study presented in this paper. An additional reason discussed by P98 is that the light at  $K$ -band is less sensitive to metallicity effects. If the slope of the Fundamental Plane is due to variations in the metallicity of the stellar populations, then it should be very different at  $K$ -band compared to optical wavelengths. If the slope of the Fundamental Plane is influenced by structural, or kinematic non-homology in ellipticals, then the slope at  $K$ -band should be similar to the slope at optical wavelengths. Both Mobasher et al. (1999) and P98 found the slope of the  $K$ -band Fundamental Plane to be similar to its optical counterparts.

The P99 data and P98 results will be used as the basis for the comparison between elliptical galaxies and the mergers presented here. Every effort has been made to measure the mergers using the same techniques and aperture sizes used in the P99 and P98 papers. All metric measurements in the paper assume a value of  $H_0 = 75 \text{ km s}^{-1} \text{ Mpc}^{-1}$ . An additional note about references in this paper; P99 refers to the elliptical galaxy data presented in Pahre (1999) such as  $\log R_{\text{eff}}$ ,  $\sigma_{\circ}$ ,  $\langle \mu_K \rangle_{\text{eff}}$ ,  $\text{Mg}_2$ , or values derived from the data, like the effective phase-space density ( $f_{\text{eff}}$ ), while

P98 refers to the analysis of the ellipticals in regards to the fitting of parameter correlations such as the Fundamental Plane as presented in Pahre et al. (1998).

## 2. Sample

### 2.1. *K*-band imaging

The 51 objects in the sample presented here were optically selected primarily from the Atlas of Peculiar Galaxies (Arp 1966), A Catalogue of Southern Peculiar Galaxies (Arp & Madore 1987), the Atlas and Catalog of Interacting Galaxies (Vorontsov-Velyaminov 1959), and the Uppsala General Catalogue (Nilson 1973). The specific selection process is detailed in Paper I. The selections were based strictly on optical morphology and according to the following criteria:

- 1) Tidal tails, loops, and shells, which are induced by strong gravitational interaction.
- 2) A single nucleus, which, based on numerical studies, marks the completion of the merger. This criteria is important because it marks the point at which the merger should begin to exhibit properties in common with elliptical galaxies.
- 3) The absence of nearby companions which may induce the presence of tidal tails and make the object appear to be in a more advanced stage of merging.
- 4) The mergers must be observable from Mauna Kea. This limited the survey to objects with declinations  $\geq -50^\circ$ .

The sample is listed in Table 1 and includes names, right ascension, declination and whether there is photometric and/or spectroscopic data for that object. Since most of the objects have multiple designations, all subsequent references to sample galaxies within the paper, tables and figures will first use the NGC designation if available, followed by the Arp or Arp-Madore (AM), UGC, VV and lastly the IC designation if no other designation is available. Unless otherwise noted, the galaxies are listed in order of Right Ascension in tables and figures. One object from this sample, AM 0612-373, has no previously recorded redshift. The redshift used to determine a distance to this galaxy was taken from the Ca triplet measurements presented in this paper.

Table 1. Merger Sample

Merger Names	Other Names	R.A. (J2000)	Dec. (J2000)	notes	data <sup>a</sup>
UGC 6	VV 806	00 <sup>h</sup> 03 <sup>m</sup> 09 <sup>s</sup>	21° 57' 37"	LIRG	I,S
NGC 34	VV 850	00 <sup>h</sup> 11 <sup>m</sup> 06 <sup>s</sup>	-12° 06' 26"	LIRG	I,S
Arp 230	IC 51	00 <sup>h</sup> 46 <sup>m</sup> 24 <sup>s</sup>	-13° 26' 32"	Shell	I
NGC 455	Arp 164, UGC 815	01 <sup>h</sup> 15 <sup>m</sup> 57 <sup>s</sup>	05° 10' 43"		I,S
NGC 828	UGC 1655	02 <sup>h</sup> 10 <sup>m</sup> 09 <sup>s</sup>	39° 11' 25"	LIRG	I
UGC 2238	...	02 <sup>h</sup> 46 <sup>m</sup> 17 <sup>s</sup>	13° 05' 44"	LIRG	I
NGC 1210	AM 0304-255	03 <sup>h</sup> 06 <sup>m</sup> 45 <sup>s</sup>	-25° 42' 59"	Shell	I,S
AM 0318-230	...	03 <sup>h</sup> 20 <sup>m</sup> 40 <sup>s</sup>	-22° 55' 53"		I
NGC 1614	Arp 186	04 <sup>h</sup> 33 <sup>m</sup> 59 <sup>s</sup>	-08° 34' 44"	LIRG	I,S
Arp 187	...	05 <sup>h</sup> 04 <sup>m</sup> 53 <sup>s</sup>	-10° 14' 51"		I
AM 0612-373	...	06 <sup>h</sup> 13 <sup>m</sup> 47 <sup>s</sup>	-37° 40' 37"		I,S
NGC 2418	Arp 165, UGC 3931	07 <sup>h</sup> 36 <sup>m</sup> 37 <sup>s</sup>	17° 53' 02"		I,S
UGC 4079	...	07 <sup>h</sup> 55 <sup>m</sup> 06 <sup>s</sup>	55° 42' 13"		I
NGC 2623	Arp 243, UGC 4509, VV 79	08 <sup>h</sup> 38 <sup>m</sup> 24 <sup>s</sup>	25° 45' 17"	LIRG	I,S
UGC 4635	...	08 <sup>h</sup> 51 <sup>m</sup> 54 <sup>s</sup>	40° 50' 09"		I,S
NGC 2655	Arp 225, UGC 4637	08 <sup>h</sup> 55 <sup>m</sup> 37 <sup>s</sup>	78° 13' 23"	Shell	I,S
NGC 2744	UGC 4757, VV 612	09 <sup>h</sup> 04 <sup>m</sup> 38 <sup>s</sup>	18° 27' 37"		I
NGC 2782	Arp 215, UGC 4862	09 <sup>h</sup> 14 <sup>m</sup> 05 <sup>s</sup>	40° 06' 49"	LIRG	I,S
NGC 2914	Arp 137, UGC 5096	09 <sup>h</sup> 34 <sup>m</sup> 02 <sup>s</sup>	10° 06' 31"		I,S
UGC 5101	...	09 <sup>h</sup> 35 <sup>m</sup> 51 <sup>s</sup>	61° 21' 11"	ULIRG	I,S
AM 0956-282	...	09 <sup>h</sup> 58 <sup>m</sup> 46 <sup>s</sup>	-28° 37' 19"		I
NGC 3256	AM 1025-433, VV 65	10 <sup>h</sup> 27 <sup>m</sup> 51 <sup>s</sup>	-43° 54' 14"	LIRG	I,S
NGC 3310	Arp 217, UGC 5786, VV 356	10 <sup>h</sup> 38 <sup>m</sup> 45 <sup>s</sup>	53° 30' 05"		I
Arp 156	UGC 5814	10 <sup>h</sup> 42 <sup>m</sup> 38 <sup>s</sup>	77° 29' 41"		I,S
NGC 3597	AM 1112-232	11 <sup>h</sup> 14 <sup>m</sup> 41 <sup>s</sup>	-23° 43' 39"		I,S
NGC 3656	Arp 155, UGC 6403, VV 22a	11 <sup>h</sup> 23 <sup>m</sup> 38 <sup>s</sup>	53° 50' 30"	Shell	I,S
NGC 3921	Arp 224, UGC 6823, VV 31	11 <sup>h</sup> 51 <sup>m</sup> 06 <sup>s</sup>	55° 04' 43"		I,S
NGC 4004	UGC 6950, VV 230	11 <sup>h</sup> 58 <sup>m</sup> 05 <sup>s</sup>	27° 52' 44"		I,S
AM 1158-333	...	12 <sup>h</sup> 01 <sup>m</sup> 20 <sup>s</sup>	-33° 52' 36"		I
NGC 4194	Arp 160, UGC 7241, VV 261	12 <sup>h</sup> 14 <sup>m</sup> 09 <sup>s</sup>	54° 31' 36"	LIRG	I,S
NGC 4441	UGC 7572	12 <sup>h</sup> 27 <sup>m</sup> 20 <sup>s</sup>	64° 48' 06"		I,S
UGC 8058	Mrk 231	12 <sup>h</sup> 56 <sup>m</sup> 14 <sup>s</sup>	56° 52' 25"	ULIRG	I

Table 1—Continued

Merger Names	Other Names	R.A. (J2000)	Dec. (J2000)	notes	data <sup>a</sup>
AM 1255-430	...	12 <sup>h</sup> 58 <sup>m</sup> 08 <sup>s</sup>	-43° 19′ 47″		I,S
AM 1300-233	...	13 <sup>h</sup> 02 <sup>m</sup> 52 <sup>s</sup>	-23° 55′ 18″	LIRG	I
NGC 5018	UGCA 335	13 <sup>h</sup> 13 <sup>m</sup> 00 <sup>s</sup>	-19° 31′ 05″	Shell	I,S
Arp 193	UGC 8387, VV 821, IC 883	13 <sup>h</sup> 20 <sup>m</sup> 35 <sup>s</sup>	34° 08′ 22″	LIRG	I,S
AM 1419-263	...	14 <sup>h</sup> 22 <sup>m</sup> 06 <sup>s</sup>	-26° 51′ 27″		I,S
UGC 9829	VV 847	15 <sup>h</sup> 23 <sup>m</sup> 01 <sup>s</sup>	-01° 20′ 50″		I,S
NGC 6052	Arp 209, UGC 10182, VV 86	16 <sup>h</sup> 05 <sup>m</sup> 12 <sup>s</sup>	20° 32′ 32″		I,S
UGC 10607	VV 852, IC 4630	16 <sup>h</sup> 55 <sup>m</sup> 09 <sup>s</sup>	26° 39′ 46″		I,S
UGC 10675	VV 805	17 <sup>h</sup> 03 <sup>m</sup> 15 <sup>s</sup>	31° 27′ 29″		I,S
NGC 6598	UGC 11139	18 <sup>h</sup> 08 <sup>m</sup> 56 <sup>s</sup>	69° 04′ 04″		I
AM 2038-382	...	20 <sup>h</sup> 41 <sup>m</sup> 13 <sup>s</sup>	-38° 11′ 36″		I,S
AM 2055-425	...	20 <sup>h</sup> 58 <sup>m</sup> 26 <sup>s</sup>	-42° 39′ 00″	LIRG	I,S
NGC 7135	AM 2146-350, IC 5136	21 <sup>h</sup> 49 <sup>m</sup> 46 <sup>s</sup>	-34° 52′ 35″		I,S
UGC 11905	...	22 <sup>h</sup> 05 <sup>m</sup> 54 <sup>s</sup>	20° 38′ 22″		I,S
NGC 7252	Arp 226, AM 2217-245	22 <sup>h</sup> 20 <sup>m</sup> 44 <sup>s</sup>	-24° 40′ 41″		I,S
AM 2246-490	...	22 <sup>h</sup> 49 <sup>m</sup> 39 <sup>s</sup>	-48° 50′ 58″	ULIRG	I,S
IC 5298	...	23 <sup>h</sup> 16 <sup>m</sup> 00 <sup>s</sup>	25° 33′ 24″	LIRG	I,S
NGC 7585	Arp 223	23 <sup>h</sup> 18 <sup>m</sup> 01 <sup>s</sup>	-04° 39′ 01″	Shell	I,S
NGC 7727	Arp 222, VV 67	23 <sup>h</sup> 39 <sup>m</sup> 53 <sup>s</sup>	-12° 17′ 35″		I,S
Elliptical					
NGC 5812	UGCA 398	15 <sup>h</sup> 00 <sup>m</sup> 55 <sup>s</sup>	-07° 27′ 26″	E0	I,S

Note. — (a) I = *K*-band imaging, S = Spectra

In addition to the mergers in the sample, an E0 elliptical galaxy, NGC 5812, was also observed. This object was selected as a “control-sample” elliptical. It was observed using the same instrument setups and analyzed in exactly the same way as the mergers presented in this paper. P99 also observed NGC 5812 at  $K$ -band, and extracted  $\sigma_o$  and  $Mg_2$  values from the literature. This makes it useful for comparing the P99 photometric results with those presented in this paper and ruling out any systematic differences which may affect comparisons between that study and this one. The photometric differences between P99 and the photometry presented here are small;  $\Delta\langle\mu_K\rangle_{\text{eff}} = 0.01$ ,  $\Delta \log R_{\text{eff}} = 0.03$ ,  $\Delta M_K = 0.02$ .

Within the merger sample there are three sub-samples, “shell ellipticals,” ultra-luminous and luminous infrared galaxies (LIRG/ULIRGs), and “normal” mergers, which are defined simply as those galaxies which are neither LIRG/ULIRGs nor shell ellipticals. Each of the sub-samples are plotted with different symbols in all figures. A more in-depth discussion of the first two sub-samples is given in Paper I.

## 2.2. Spectroscopy

The optical spectroscopic observations consist of a sub-sample of 38 objects taken from the  $K$ -band imaging sample. The sub-sample was not selected based on any particular criteria. The goal of the spectroscopic campaign was to obtain velocity dispersions for every galaxy in the sample. Unfortunately, due to limitations of time, only 38/51 objects in the sample could be observed. The 38 objects were observed in no particular order. In addition to the optical spectra, two mergers, NGC 1614 and NGC 2623, were observed in the infrared at  $2.29 \mu\text{m}$  which corresponds to the CO molecular absorption line.

## 3. Observations

### 3.1. $K$ -band imaging

Near-infrared images were obtained using the Quick Infrared Camera (QUIRC)  $1024 \times 1024$  pixel HgCdTe infrared array (Hodapp et al. 1996) at  $f/10$  focus on the University of Hawaii 2.2 meter telescope. The field of view of the QUIRC array is  $193'' \times 193''$  with a plate scale of  $0.189'' \text{ pixel}^{-1}$ . Exposures from QUIRC were obtained by nodding between the source and a blank field of sky. The on-target observations were dithered so as to remove any array defects in the final processing. The infrared photometric standards were selected based on proximity to the targets in Right Ascension and Declination. Multiple observations of standard stars were taken before and after target observations. Standards were selected from Persson et al. (1998), Carter & Meadows (1995), Hunt et al. (1998), and Hawarden et al. (2001), which includes the UKIRT faint standards. The median seeing for the observations was  $0''.8$

The  $K$  filter used in this survey for all but two objects conforms to the new Mauna Kea Infrared

Filter Set (Tokunaga, Simons, & Vacca 2002). One object, UGC 6 was observed with the  $K'$  filter (Wainscoat & Cowie 1992) and has been converted to  $K$  using their conversion equation. Another object, IC 5298, was observed with an older  $K$  filter with similar properties to the Mauna Kea  $K$  filter. No conversion was made and it is assumed that  $K_{old} \simeq K_{MaunaKea}$ . Table 2 lists the observation log for each object, including the total integration time and the measured seeing for each object.

Table 2. *K*-band Photometry Observation Log

Merger Name	Integration Time (sec)	seeing ( $''$ )
UGC 6	3210	0.90
NGC 34	3300	0.94
Arp 230	2325	1.45
NGC 455	2250	0.90
NGC 828	2580	1.19
UGC 2238	3480	0.98
NGC 1210	2820	0.68
AM 0318-230	3660	0.98
NGC 1614	2730	0.64
Arp 187	3150	0.92
AM 0612-373	2160	1.09
NGC 2418	3600	0.68
UGC 4079	3600	0.58
NGC 2623	3390	0.64
UGC 4635	3480	0.64
NGC 2655	1800	0.92
NGC 2744	3600	0.60
NGC 2782	3000	0.62
NGC 2914	1800	0.81
UGC 5101	2700	1.02
AM 0956-282	3600	0.62
NGC 3256	2925	1.02
NGC 3310	2940	0.90
Arp 156	2400	0.86
NGC 3597	3300	0.81
NGC 3656	3150	0.58
NGC 3921	3645	0.88
NGC 4004	1560	0.86
AM 1158-333	3600	0.69
NGC 4194	3600	0.62
NGC 4441	1440	0.86
UGC 8058	1170	0.62

Table 2—Continued

Merger Name	Integration Time (sec)	seeing (")
AM 1255-430	3420	0.90
AM 1300-233	1200	0.62
NGC 5018	2025	0.66
Arp 193	2625	0.62
AM 1419-263	3600	0.79
UGC 9829	3600	0.62
NGC 6052	3600	0.71
UGC 10607	3360	0.75
UGC 10675	3600	0.62
NGC 6598	2700	0.66
AM 2038-382	1920	0.69
AM 2055-425	2880	1.02
NGC 7135	2520	0.69
UGC 11905	3000	0.81
NGC 7252	3360	0.90
AM 2246-490	2520	1.17
IC 5298	3240	0.62
NGC 7585	2040	0.92
NGC 7727	3240	0.83
Elliptical		
NGC 5812	2400	1.41

### 3.2. Optical Spectroscopy

The optical spectroscopic observations were obtained with the Echellette Spectrograph and Imager (Sheinis et al. 2002) at the W. M. Keck-II 10-meter observatory. The spectrograph covers the wavelength range from 3927-11068 Å. The observations were made in the echelle mode using the  $0''.5 \times 20''$  slit. In this mode, ten orders are projected onto a 2048×4096 CCD. ESI has a resolution of  $11.2 \text{ km s}^{-1} \text{ pixel}^{-1}$ . The  $0''.5$  slit projects to 3.24 pixels, providing a resolution of  $R \simeq 36.2 \text{ km s}^{-1}$  or  $R \simeq 8200$ . The slit Position Angle was placed along the major axis of each galaxy. The P.A. of the major axis was measured using the *K*-band data and is listed for each galaxy in the spectroscopic observation log of Table 3, along with the total integration time for each object. Dome flats and calibration arcs were observed at the beginning and end of each night. Dome flats were selected over internal flats for use in the reduction process in order to correct the high-frequency fringing which occurs in the higher orders of the spectra (beyond  $\lambda \simeq 7100 \text{ Å}$ ). The calibration arcs consisted of separate exposures containing Cu-Ar lines and Hg-Xe-Ne lines. Spectrophotometric standards were selected from Massey & Gronwall (1990) for objects with northern declinations and from Hamuy et al. (1994) for southern declinations. The standards were observed at several intervals throughout each night. In addition to the spectrophotometric standards, giant stars covering the spectral range from G0III to M3III, and two super-giants of class M1Iab and M2Iab were observed with the same instrumental setup for use as template stars for the kinematic analysis. The observed template stars are listed in Table 4.

Table 3. Merger Spectroscopic Observation Log

Merger Name	Integration Time (sec)	P.A. °
ESI Merger Observations		
UGC 6	540	90.0
NGC 34	1200	-41.0
NGC 455	1800	-30.0
NGC 1210	300	-41.0
NGC 1614	1800	32.9
AM 0612-373	1800	40.0
NGC 2418	1800	30.8
NGC 2623	1800	64.1
UGC 4635	1800	49.8
NGC 2655	1800	83.8
NGC 2782	1800	90.0
NGC 2914	1800	20.5
UGC 5101	1800	83.0
NGC 3256	629	0.0
Arp 156	3600	-61.8
NGC 3597	1800	76.7
NGC 3656	900	-8.7
NGC 3921	1800	29.5
NGC 4004	1800	-12.0
NGC 4194	1800	-20.0
NGC 4441	1800	2.0
AM 1255-430	2700	-77.2
NGC 5018	1140	90.0
Arp 193	3600	-39.3
AM 1419-263	1800	69.0
UGC 9829	1800	-15.0
NGC 6052	1800	71.5
UGC 10607	1800	0.0
UGC 10675	1800	90.0

Table 3—Continued

Merger Name	Integration Time (sec)	P.A. ◦
AM 2038-382	1200	-45.0
AM 2055-425	1200	-35.0
NGC 7135	1800	0.0
UGC 11905	1200	49.5
NGC 7252	1800	-60.0
AM 2246-490	1200	-5.0
IC 5298	900	29.7
NGC 7585	900	-70.0
NGC 7727	900	90.0
ESI Elliptical Observations		
NGC 5812	900	61.4
NIRSPEC Merger Observations		
NGC 1614	900	32.9
NGC 2623	850	64.1

Table 4. Template Stars

Name	R.A.	Dec.	Type
ESI Observations			
HD 232766	03 <sup>h</sup> 13 <sup>m</sup> 57 <sup>s</sup>	54° 56′ 08″	M1Iab
HD 283778	04 <sup>h</sup> 42 <sup>m</sup> 58 <sup>s</sup>	27° 54′ 51″	M0III
BD -15 1319	06 <sup>h</sup> 15 <sup>m</sup> 01 <sup>s</sup>	-15° 52′ 49″	K5III
HD 260158	06 <sup>h</sup> 36 <sup>m</sup> 14 <sup>s</sup>	29° 31′ 15″	K0III
HD 50567	06 <sup>h</sup> 52 <sup>m</sup> 35 <sup>s</sup>	-29° 30′ 26″	M2-3III
HD 97646	11 <sup>h</sup> 14 <sup>m</sup> 02 <sup>s</sup>	-12° 47′ 38″	K5III
HD 99724	11 <sup>h</sup> 28 <sup>m</sup> 15 <sup>s</sup>	-18° 38′ 32″	K3III
HD 99814	11 <sup>h</sup> 28 <sup>m</sup> 52 <sup>s</sup>	-16° 35′ 41″	M3III
HD 100059	11 <sup>h</sup> 30 <sup>m</sup> 43 <sup>s</sup>	-19° 53′ 46″	K0III
HD 100347	11 <sup>h</sup> 32 <sup>m</sup> 39 <sup>s</sup>	-18° 52′ 15″	G8III
HD 100745	11 <sup>h</sup> 35 <sup>m</sup> 30 <sup>s</sup>	-19° 31′ 59″	M0III
GSC 02146-01226	19 <sup>h</sup> 38 <sup>m</sup> 04 <sup>s</sup>	27° 58′ 41″	G5III
BD +19 4103	19 <sup>h</sup> 39 <sup>m</sup> 18 <sup>s</sup>	20° 10′ 59″	M2Iab
HD 332389	19 <sup>h</sup> 40 <sup>m</sup> 06 <sup>s</sup>	29° 42′ 58″	G0III
NIRSPEC Observations			
HD 284318	04 <sup>h</sup> 18 <sup>m</sup> 59 <sup>s</sup>	22° 08′ 28″	K0III
Other CO 2.29 $\mu\text{m}$ Templates <sup>a</sup>			
$\alpha$ Orionis	05 <sup>h</sup> 55 <sup>m</sup> 10 <sup>s</sup>	07° 24′ 25″	M1Iab
$\lambda$ Dra	11 <sup>h</sup> 31 <sup>m</sup> 24 <sup>s</sup>	69° 19′ 51″	M0III
$\alpha$ Boo	14 <sup>h</sup> 15 <sup>m</sup> 39 <sup>s</sup>	19° 10′ 56″	K1.5III
Rx Boo	14 <sup>h</sup> 24 <sup>m</sup> 11 <sup>s</sup>	25° 42′ 13″	M7.5III

Note. — (a) from Wallace & Hinkle 1996

### 3.3. 2.29 $\mu\text{m}$ CO spectroscopy

Infrared spectroscopic observations centered on the 2.29  $\mu\text{m}$  CO feature were obtained with the NIRSPEC spectrograph (McLean et al. 1998) on the W. M. Keck-II 10-meter telescope. The infrared spectrograph contains a  $1024 \times 1024$  ALADDIN InSb array. NIRSPEC covers the wavelength range from 0.95-5.5  $\mu\text{m}$ . The observations were made in the echelle mode using the  $0''.432 \times 24''$  slit. This gives a resolution of  $R \simeq 12 \text{ km s}^{-1}$  or  $R \simeq 25,000$ . NIRSPEC contains only a single echelle grating and a single cross-disperser. This requires 25 different grating settings to span the entire 0.95-5.5  $\mu\text{m}$  wavelength range. The NIRSPEC-7 filter was used, which transmits light between 1.839-2.630  $\mu\text{m}$  and is dispersed over 13 orders. Because the area of the array is smaller than the area onto which the orders are dispersed, only 6-7 non-contiguous orders are projected onto the array at any given time. The actual wavelength range of any particular order projected onto the array is  $\lambda \simeq 0.33 \mu\text{m}$ . The grating settings were set to the redshifted CO absorption line for the galaxies and standards, and 2.29  $\mu\text{m}$  for the template star. The slit Position Angle was placed along the major axis of each galaxy. The P.A. was determined using the  $K$ -band data and is listed in Table 3 for each galaxy. Due to the redshift of the galaxies observed, and the wavelength range of the orders, the CO feature could not be centered in the middle of the array, but was shifted slightly right of center. Since the galaxies were larger than the length of the slit, the observations required nodding to a blank area of sky in order to subtract the sky lines and background. Observations were done in an A-B-B-A pattern. In addition to telluric standards, a K0III star was observed with the same instrumental setup for use as template star for the kinematic analysis. Observations of telluric standards and template star observations were made by nodding along the slit. Ne-Ar-Xe-Kr arcs and internal flats were taken after observations of each object and standard star.

## 4. Data Reduction and Analysis

### 4.1. $K$ -band imaging

The data set was reduced using IRAF. The global photometric parameters  $R_{\text{eff}}$ ,  $\langle \mu_K \rangle_{\text{eff}}$ , and  $M_K$  were measured using circular apertures. The IRAF ELLIPSE package in STSDAS was used to extract the total flux in circular apertures. Circular apertures were selected over elliptical apertures because they are less sensitive to sky-subtraction errors and to match the method used by P99.

The ELLIPSE fitting was conducted by first using IMEXAMINE to find the maximum brightness at the center of the galaxy. The center position was then held fixed. The radius of each isophote was increased in linear steps of size equal to the seeing. The seeing estimates for the galaxies were obtained by measuring the FWHM of high signal-to-noise (S/N) stars in the field and taking the average value. Stars in the field were masked and those pixels were ignored in the isophote fitting and flux measurement. Only the number of pixels (area in pixels) and the total flux in each circular aperture from the circular apertures were used from ELLIPSE.

The output from ELLIPSE was put into an IDL program which computes the surface brightness, S/N and errors at each circular aperture radius. The program fits a de Vaucouleurs  $r^{1/4}$  profile to each galaxy using a Levenberg-Marquardt non-linear least squares minimization technique to achieve a good fit (Press et al. 1992). All data points were used in the fits. The summed total flux in the circular apertures was used to compute  $M_K$ .

It is important to make clear the distinction in terminology between  $r_{\text{eff}}$  and  $R_{\text{eff}}$ . The former refers to the effective radius in arcseconds, whereas the latter is a metric value in kiloparsecs.  $R_{\text{eff}}$  will be used throughout the rest of the paper. No corrections to the  $K$ -band data have been made for galactic extinction. Since the reddening at  $K$  is very small, any such corrections, even for objects at low galactic latitude would be negligible and well within the errors from standard star calibrations. Table 5 lists the extracted photometric properties of the mergers, including  $R_{\text{eff}}$ ,  $\langle\mu_K\rangle_{\text{eff}}$ , and  $M_K$ .

Table 5. *K*-band Photometric Parameters

Merger Name	Log $R_{\text{eff}}$ (kpc)	$\langle \mu_K \rangle_{\text{eff}}$ (mag arcsec $^{-2}$ )	$M_K$ (mag)
UGC 6	0.145	15.18	-24.01
NGC 34	-0.078	13.24	-24.61
Arp 230	0.034	16.71	-21.75
NGC 455	0.523	16.32	-24.64
NGC 828	0.545	15.69	-25.36
UGC 2238	0.151	14.44	-24.58
NGC 1210	0.385	16.64	-23.72
AM 0318-230	0.561	16.10	-25.09
NGC 1614	0.227	14.92	-24.74
Arp 187	0.640	16.33	-25.25
AM 0612-373	0.673	16.08	-25.65
NGC 2418	0.682	16.40	-25.31
UGC 4079	0.562	17.47	-23.78
NGC 2623	0.120	14.83	-24.22
UGC 4635	0.395	15.73	-24.71
NGC 2655	0.058	14.96	-23.70
NGC 2744	0.536	18.11	-22.83
NGC 2782	0.519	17.04	-23.83
NGC 2914	0.143	15.82	-23.51
UGC 5101	0.028	12.82	-25.50
AM 0956-282	0.339	19.25	-20.50
NGC 3256	0.254	14.83	-24.72
NGC 3310	-0.153	15.51	-22.07
Arp 156	0.843	16.96	-25.81
NGC 3597	-0.082	14.21	-23.72
NGC 3656	0.406	16.62	-23.70
NGC 3921	0.538	16.18	-25.13
NGC 4004	0.501	17.90	-22.89
AM 1158-333	0.150	16.58	-22.61
NGC 4194	-0.246	14.03	-23.21
NGC 4441	0.186	16.37	-22.98

Table 5—Continued

Merger Name	Log $R_{\text{eff}}$ (kpc)	$\langle \mu_K \rangle_{\text{eff}}$ (mag arcsec $^{-2}$ )	$M_K$ (mag)
UGC 8058	-0.087	10.68	-27.55
AM 1255-430	0.714	17.11	-24.93
AM 1300-233	0.641	16.96	-24.65
NGC 5018	0.418	15.33	-25.15
Arp 193	0.198	15.10	-24.40
AM 1419-263	0.557	16.25	-24.94
UGC 9829	0.820	17.68	-24.96
NGC 6052	0.683	17.96	-23.55
UGC 10607	0.202	14.15	-25.20
UGC 10675	0.164	14.66	-24.80
NGC 6598	0.784	16.75	-25.51
AM 2038-382	0.249	15.12	-24.70
AM 2055-425	0.320	14.93	-25.08
NGC 7135	0.639	17.47	-23.95
UGC 11905	0.277	15.26	-24.51
NGC 7252	0.403	15.53	-24.84
AM 2246-490	0.619	16.01	-25.52
IC 5298	0.281	14.90	-24.92
NGC 7585	0.648	16.52	-24.98
NGC 7727	0.357	15.86	-24.23
Elliptical			
NGC 5812	0.252	15.52	-24.08

## 4.2. Optical Spectroscopy

Only the orders containing the Ca triplet absorption line at  $\lambda \simeq 8500 \text{ \AA}$  (order 7) and the Mg<sub>2</sub> absorption line at  $\lambda = 5128 \text{ \AA}$  (orders 11 and/or 12 depending on how far the line and continuum are redshifted) were analyzed for the data presented in this paper. The spectroscopic data were reduced using IRAF. The spectra were bias-subtracted, and cosmic-rays were identified and fixed in each image. A bright spectrophotometric standard was used to trace the curved orders before extraction. The spectra were then extracted in “strip” mode with the APALL task. This produced a two-dimensional, rectified spectrum. Dome flats and calibration arcs were also extracted in the same manner. The data were then reduced in a manner similar to that for long-slit spectra. Each order was divided by the corresponding normalized flat for that order. One-dimensional spectra were extracted in an aperture of diameter equivalent to  $1.53 h^{-1}_{75} \text{ kpc}$  for each object. This aperture size was selected to match the size used in the near-infrared Fundamental Plane study by P98 and P99. The order containing the Ca triplet spectra was wavelength calibrated using a Hg-Ne-Xe lamp spectra. The orders containing the Mg<sub>2</sub> line and continuum were wavelength calibrated using a Cu-Ar lamp spectra. The rms of the residuals of the wavelength solutions were  $0.09 \text{ \AA}$  or better. A sky spectrum was measured at both edges of the slit. A 2nd order Legendre polynomial was fit to the background and then subtracted from the spectra. Next, the extracted spectra were corrected to a heliocentric rest velocity. The spectra were then flux-calibrated and continuum normalized by fitting a 5th order spline3 function to the continuum. The Ca triplet line lies in order 7, which covers the wavelength range from  $8117\text{-}9366 \text{ \AA}$ . This order is affected by strong H<sub>2</sub>O telluric absorption longwards of  $9000 \text{ \AA}$ . Depending on the redshift of the object, the Ca triplet lines can lie within this feature. As a result, the spectra were corrected for telluric absorption using the IRAF task TELLURIC.

### 4.2.1. Ca triplet

The spectra were convolved with a Gaussian equal to the number of pixels in one resolution element. The measurements of the velocity dispersion were carried out using a direct template fitting routine. The direct fitting routine occurs in pixel-space, and is based on the methods first described by Rix & White (1992). The advantage to this method is that it is straightforward to mask out unwanted features and compute a minimized chi-square over an exact wavelength range. It is more computationally intensive than other techniques such as the cross-correlation method (Tonry & Davis 1979) and the Fourier quotient method (e.g. Sargent et al. (1978)). However, it has several advantages over these techniques. First, there is no need to worry about the ends of the spectrum, which can introduce significant high-frequency noise in Fourier space. Second, absorption features in the spectrum other than those under analysis do not interact with each other as they do in Fourier space. Finally, template mismatch errors are significantly reduced in pixel space.

The process of pixel-space fitting is simple and straightforward. The template star is broadened

until the  $\chi_\nu^2$  of the fit reaches a minimum. Thus the best-fit parameters are those which minimize the  $\chi_\nu^2$  for the difference between the broadened template and galaxy. Recently, Barth, Ho, & Sargent (2002) defined an optimal fitting region to use for both the Mg *Ib* and Ca triplet absorption features. The same fitting region of 8480-8690 Å has been adopted here. However, unlike Barth, Ho, & Sargent, who assumed a Gaussian profile for the line-of-sight velocity distribution (LOSVD), a Gauss-Hermite series polynomial was used to parameterize the Ca triplet line profiles. The Gauss-Hermite series is described in detail by van der Marel & Franx (1993). The Gauss-Hermite function is a modified Gaussian with additional parameters that parameterize departures from a Gaussian shape. Briefly, the form of the fitting function is:

$$L(v) = \gamma \frac{\alpha(\omega)}{\sigma} [1 + h_3 H_3(\omega) + h_4 H_4(\omega)] \quad (1)$$

where  $\omega \equiv (v - v_o)/\sigma$  and

$$\alpha(\omega) \equiv \frac{1}{\sqrt{2\pi}} e^{-\omega^2/2} \quad (2)$$

$$H_3(\omega) \equiv \frac{1}{\sqrt{6}} (2\sqrt{2}\omega^3 - 3\sqrt{2}\omega) \quad (3)$$

$$H_4(\omega) \equiv \frac{1}{\sqrt{24}} (4\omega^4 - 12\omega^2 + 3) \quad (4)$$

When  $h_3 = h_4 = 0$ , the Gauss-Hermite series becomes a normal Gaussian profile. The fitting function has five parameters: the line strength  $\gamma$ , which measures the ratio of the equivalent width of the galaxy to that of the template star; the mean recessional velocity  $v_o$ , the central velocity dispersion  $\sigma_o$ , the skewness  $h_3$ , and kurtosis  $h_4$ . Skewness parameterizes the asymmetric departures from a Gaussian, while the kurtosis parameterizes the symmetric departures from a Gaussian. Crudely, a positive  $h_3$  shifts the Gaussian to the left, a negative  $h_3$  shifts the Gaussian to the right; while a positive  $h_4$  makes the peak of the Gaussian more triangular and a negative  $h_4$  squashes the peak of the Gaussian downwards.

The fitting program uses a Levenberg-Marquardt non-linear least squares minimization technique to achieve a good fit (Press et al. 1992). The five parameters,  $\gamma$ ,  $v_o$ ,  $\sigma$ ,  $h_3$ , and  $h_4$  are simultaneously fit to the data over the specified wavelength range. A single stellar population template was used in the fitting. All of the stellar templates listed in Table 4 were fit to each galaxy. The best fitting template for each galaxy was chosen based on the reduced chi-square and rms of the fit. The best-fit template star used for each galaxy is listed in Table 6 along with the results of the fit. The parameters listed were extracted using the best fitting template.

The errors shown in Table 6 are not absolute, and are provided more as reasonable estimates. The error analysis was conducted by testing various limits on the fitting process. First, Monte Carlo simulations were conducted to test the fitting program. The testing was based on 100 realizations of a template star convolved with a Gauss-Hermite polynomial of known properties with

random noise added. This altered template star was used as a “test galaxy,” to determine whether the fitting program could recover the input parameters of  $\gamma$ ,  $v_o$ ,  $\sigma_o$ ,  $h_3$ , and  $h_4$ . Next, a second template star of identical stellar type was used to recover the input parameters of the “test galaxy.” The spread in errors from the Monte Carlo simulations were found to be nearly the same as the fitting errors determined by the program. Finally, template mis-match was tested by investigating the spread in the derived parameters from using different template stars. Only template stars which produced fits within  $2 \times \chi_\nu^2$  of the best-fitting template were used to test each galaxy. The results show that template mis-match produced the largest errors in the fitting. The errors listed in Table 6 for each parameter are the standard deviations of the derived parameters for the range of template stars used to test the template mis-match. The spectrum for each galaxy is shown in Appendix A. The solid line is the galaxy spectrum and the overplotted dashed line is the convolved best-fitting template.

Table 6. Spectroscopic Parameters

Merger Name	$\sigma_{\circ}$ (km s <sup>-1</sup> )	$V_{\odot}$ (km s <sup>-1</sup> )	$\gamma$	$h_3$	$h_4$	Best-fit Template star/type
ESI Observations						
UGC 6	220 ± 10	6579 ± 1	0.906 ± 0.005	-0.013 ± 0.009	0.185 ± 0.018	HD 332389 G0III
NGC 34	201 ± 8	5881 ± 2	1.054 ± 0.014	0.000 ± 0.006	-0.079 ± 0.030	HD 332389 G0III
NGC 455	234 ± 7	5827 ± 1	0.970 ± 0.012	-0.005 ± 0.004	0.069 ± 0.026	HD 100059 K0III
NGC 1210	247 ± 6	3878 ± 7	0.953 ± 0.011	0.052 ± 0.016	0.116 ± 0.021	HD 283778 M0III
NGC 1614	146 ± 12	4769 ± 1	0.921 ± 0.006	-0.031 ± 0.006	0.136 ± 0.020	HD 332389 G0III
AM 0612-373	303 ± 8	9721 ± 2	0.974 ± 0.003	-0.047 ± 0.009	0.101 ± 0.010	HD 99724 K3III
Arp 165	288 ± 10	5037 ± 1	0.962 ± 0.009	0.017 ± 0.003	0.091 ± 0.021	HD 100347 G8III
NGC 2623	191 ± 7	5549 ± 1	0.957 ± 0.008	-0.014 ± 0.006	0.106 ± 0.020	HD 100347 G8III
UGC 4635	251 ± 7	8722 ± 1	0.993 ± 0.009	0.002 ± 0.003	0.056 ± 0.019	HD 100347 G8III
NGC 2655	169 ± 11	1400 ± 1	0.995 ± 0.004	0.013 ± 0.004	0.043 ± 0.011	HD 100347 G8III
NGC 2782	196 ± 8	2543 ± 2	0.946 ± 0.007	-0.003 ± 0.009	0.135 ± 0.019	HD 100347 G8III
NGC 2914	186 ± 4	3159 ± 1	1.010 ± 0.019	-0.001 ± 0.005	0.014 ± 0.034	HD 100059 K0III
UGC 5101	287 ± 11	11802 ± 2	0.983 ± 0.009	0.000 ± 0.006	0.096 ± 0.021	HD 100347 G8III
NGC 3256	241 ± 16	2795 ± 8	0.849 ± 0.003	-0.035 ± 0.030	0.348 ± 0.010	HD 100347 G8III
Arp 156	288 ± 8	10738 ± 4	0.994 ± 0.006	0.162 ± 0.007	0.071 ± 0.013	HD 260158 K0III
NGC 3597	174 ± 9	3500 ± 1	0.913 ± 0.009	-0.047 ± 0.007	0.185 ± 0.024	HD 100347 G8III
NGC 3656	132 ± 18	2890 ± 11	1.035 ± 0.016	0.108 ± 0.045	-0.057 ± 0.032	HD 332389 G0III
NGC 3921	222 ± 5	5896 ± 1	1.010 ± 0.014	-0.115 ± 0.007	0.011 ± 0.027	HD 100347 G8III
NGC 4004	33 ± 2	3368 ± 1	0.998 ± 0.024	0.001 ± 0.019	0.014 ± 0.041	HD 100347 G8III
NGC 4194	116 ± 7	2501 ± 1	0.891 ± 0.004	-0.086 ± 0.008	0.247 ± 0.014	HD 100347 G8III
NGC 4441	139 ± 6	2722 ± 1	0.923 ± 0.012	-0.060 ± 0.009	0.172 ± 0.029	HD 100347 G8III

Table 6—Continued

Merger Name	$\sigma_{\circ}$ (km s <sup>-1</sup> )	$V_{\odot}$ (km s <sup>-1</sup> )	$\gamma$	$h_3$	$h_4$	Best-fit Template star/type
AM 1255-430	243 ± 3	8984 ± 2	1.017 ± 0.008	-0.170 ± 0.010	0.039 ± 0.016	HD 99724 K3III
NGC 5018	222 ± 3	2816 ± 1	0.997 ± 0.003	-0.008 ± 0.006	0.035 ± 0.007	HD 100059 K0III
Arp 193	172 ± 8	6985 ± 3	1.001 ± 0.008	-0.032 ± 0.008	0.005 ± 0.020	HD 332389 G0III
AM 1419-263	260 ± 6	6758 ± 1	0.978 ± 0.005	0.021 ± 0.003	0.070 ± 0.011	HD 100059 K0III
UGC 9829	134 ± 4	8465 ± 1	0.980 ± 0.009	-0.013 ± 0.007	0.074 ± 0.018	HD 100059 K0III
NGC 6052	80 ± 5	4739 ± 1	0.881 ± 0.005	-0.016 ± 0.007	0.250 ± 0.017	HD 100347 G8III
UGC 10607	211 ± 5	10376 ± 2	1.002 ± 0.010	-0.045 ± 0.008	0.037 ± 0.021	HD 100347 G8III
UGC 10675	177 ± 6	10179 ± 2	0.971 ± 0.005	0.034 ± 0.005	0.106 ± 0.013	HD 100347 G8III
AM 2038-382	257 ± 8	6092 ± 2	0.992 ± 0.012	-0.049 ± 0.006	0.040 ± 0.026	HD 100347 G8III
AM 2055-425	185 ± 6	12890 ± 2	1.054 ± 0.009	-0.007 ± 0.007	-0.085 ± 0.020	HD 332389 G0III
NGC 7135	277 ± 9	2644 ± 1	0.983 ± 0.010	0.000 ± 0.003	0.070 ± 0.022	HD 100347 G8III
UGC 11905	222 ± 9	7456 ± 1	0.957 ± 0.009	-0.014 ± 0.014	0.110 ± 0.022	HD 100347 G8III
NGC 7252	166 ± 5	4792 ± 1	0.968 ± 0.015	-0.023 ± 0.007	0.076 ± 0.030	HD 100347 G8III
AM 2246-490	267 ± 7	12901 ± 2	0.967 ± 0.007	-0.060 ± 0.008	0.103 ± 0.016	HD 100347 G8III
IC 5298	193 ± 6	8221 ± 1	0.961 ± 0.006	-0.065 ± 0.004	0.118 ± 0.015	HD 100347 G8III
NGC 7585	211 ± 4	3539 ± 1	0.965 ± 0.003	-0.021 ± 0.009	0.085 ± 0.006	HD 100059 K0III
NGC 7727	231 ± 5	1868 ± 2	0.968 ± 0.003	0.017 ± 0.005	0.089 ± 0.008	HD 99724 K3III
Elliptical						
NGC 5812	241 ± 4	1970 ± 2	0.967 ± 0.003	0.000 ± 0.006	0.099 ± 0.005	HD 100059 K0III
NIRSPEC Observations						

Table 6—Continued

Merger Name	$\sigma_{\circ}$ (km s <sup>-1</sup> )	$V_{\odot}$ (km s <sup>-1</sup> )	$\gamma$	$h_3$	$h_4$	Best-fit Template star/type
NGC 1614	143 ± 12	4779 ± 5	1.068 ± 0.063	-0.116 ± 0.024	0.065 ± 0.135	Rx Boo M7.5III
NGC 2623	139 ± 19	5555 ± 17	1.155 ± 0.086	0.078 ± 0.021	-0.186 ± 0.164	λ Dra M3III

#### 4.2.2. $Mg_2$

The  $Mg_2$  absorption feature at  $5178 \text{ \AA}$  was measured using the index bandpass and pseudo-continua defined by Worthey et al. (1994). The index bandpass is given as  $5154.125\text{-}5196.625 \text{ \AA}$ . The blue pseudo-continuum is  $4895.125\text{-}4957.625$  and the red pseudo-continuum is  $5301.125\text{-}5366.125$ . The index is measured in units of magnitude. This bandpass is defined as part of the Lick/IDS system. It is defined by the use of the Lick Observatory image dissector scanner (IDS), which has an  $8.4 \text{ \AA}$  resolution at that wavelength range. The spectra observed using the Lick IDS spectrograph were not flux-calibrated, or corrected for instrument response. The indices were measured on the original spectra (Faber et al. 1985). A line representing the pseudo-continuum was drawn between the midpoints of the two sidebands and the flux difference between this line and the central bandpass flux determines the index. In order to convert to the Lick/IDS system from another spectrograph, it is necessary to first convolve the spectra to the same resolution and then calibrate the indices by observing “standards,” which are any stars previously observed on the Lick IDS spectrograph.

The  $Mg_2$  magnitudes listed in Table 7 are raw magnitudes because they have not been fully converted to the Lick/IDS system. The spectra were convolved with a Gaussian to smooth the resolution to  $8.4 \text{ \AA}$ , but unfortunately, no stars previously observed with the Lick IDS spectrograph were observed with ESI. Furthermore, the prescription for data reduction as defined by Faber et al. produced problems with the ESI data. Measurements made on the raw ESI data produced spurious and often negative magnitudes (even though the  $Mg_2$  absorption feature was present). This is due to the shape of the spectral response of ESI in those orders. Instead, the spectra were flux calibrated in order to remove the spectral response of the instrument. Brodie & Huchra (1990) compared results between flux calibrated and non flux calibrated indices and found a negligible difference. A comparison of the  $Mg_2$  index for NGC 5812 extracted from the literature by P99 (and calibrated onto the Lick system) and measured with ESI, using the same aperture size, shows a difference of  $\simeq 0.02 \text{ mag}$ .

Table 7. Mg<sub>2</sub> Indices

Merger Name	Mg <sub>2</sub> (mag) <sup>a</sup>
UGC 6	0.06
NGC 34	0.04
NGC 455	0.22
NGC 1210	0.34
NGC 1614	0.06
AM 0612-373	0.21
NGC 2418	0.30
NGC 2623	0.08
UGC 4635	0.29
NGC 2655	0.19
NGC 2782	0.10
NGC 2914	0.26
UGC 5101	0.13
NGC 3256	0.03
Arp 156	0.26
NGC 3597	0.06
NGC 3656	0.12
NGC 3921	0.02
NGC 4004	0.06
NGC 4194	0.06
NGC 4441	0.08
AM 1255-430	0.13
NGC 5018	0.17
Arp 193	0.11
AM 1419-263	0.26
UGC 9829	0.20
NGC 6052	0.08
UGC 10607	0.14
UGC 10675	0.04
AM 2038-382	0.06
AM 2055-425	0.04
NGC 7135	0.29

Table 7—Continued

Merger Name	Mg <sub>2</sub> (mag) <sup>a</sup>
UGC 11905	0.10
NGC 7252	0.09
AM 2246-490	0.05
IC 5298	0.13
NGC 7585	0.21
NGC 7727	0.28
Elliptical	
NGC 5812	0.29

Note. — (a) Raw Mg<sub>2</sub> indices. They have not been fully calibrated to the Lick/IDS system.

### 4.3. 2.29 $\mu\text{m}$ CO spectroscopy

Only the order containing the CO absorption feature was analyzed for the data presented in this paper. The spectroscopic data were reduced using IRAF. A bad-pixel mask was created using one of the dark frames and used to mask bad pixels and cosmetic defects on the array. The data were then pair-subtracted to remove background night-sky lines. Bright standard stars were used to trace the curved orders before extraction. The spectra were then extracted in “strip” mode with the APALL task. This produced a two-dimensional, spectrum. Flats and calibration arcs were also extracted in the same manner. The data were then reduced in a manner similar to that for long-slit spectra. Each order was divided by the corresponding normalized flat for that order.

In addition to a slight curve present in the orders, the spectral lines are also curved along both the spatial and dispersion axes. The orders were straightened in IRAF by measuring and computing the curvature of the Ne-Ar-Xe-Kr arc lines in the arc calibration frames and applying the results to the science data frames. The spectra were then extracted in an aperture of diameter equivalent to  $1.53 h^{-1}_{75}$  kpc for each object. This aperture size was selected to match the size used in the near-infrared Fundamental Plane study by P98 and P99. The slit width used was  $0''.432$ , which is very close to the size used for the ESI data. The order was then wavelength calibrated using the Ne-Ar-Xe-Kr arc. A 2nd order Legendre polynomial was fit to the background and then subtracted from the spectra in order to remove any residual background lines that were not properly pair-subtracted. Next, the extracted spectra were corrected to a heliocentric rest velocity. The spectra were then divided by an A0V telluric standard. This removes telluric atmospheric absorption features which can be quite strong in the near-infrared. The spectra were not flux calibrated. The continuum was then normalized by fitting a 1st-order Legendre polynomial to the blue-ward side of the CO feature. This was done because there is no continuum red-ward of the CO feature.

The data analysis was identical the methods described under the ESI optical spectroscopy section above. The wavelength of the analysis was restricted to a range of 2.2775-2.3005  $\mu\text{m}$ . This was selected because it was found to be the largest wavelength range in common between the galaxies observed and the standard stars. The K0III template star observed with NIRSPEC proved to be inadequate in the fitting routine. The CO feature in the template star was too shallow compared to the depth of feature in the target galaxies. As a result additional template stars were taken from the high-resolution *K*-band spectral atlas of ordinary cool stars by Wallace & Hinkle (1996). Their data was obtained with a Fourier transform spectrograph at the Kitt Peak Mayall 4-meter telescope. The resolution was  $R \geq 45,000$ . The data were then smoothed to the resolution of NIRSPEC by convolving them with a Gaussian. Table 4 lists the template stars used from Wallace & Hinkle. The best fit template star used for the CO absorption measurements are listed in Table 6 for the two galaxies observed. The plotted spectrum for each galaxy is shown in Appendix A.

## 5. Results

### 5.1. The Near-Infrared Fundamental Plane

Figure 1 shows the  $K$ -band Fundamental Plane of elliptical galaxies with the mergers overplotted. The dotted line is the Fundamental Plane derived from P98. The mergers are plotted in this figure using the photometric data from Table 5 and the kinematic data from Table 6. The filled circles are “normal” mergers, the open circles are the LIRG/ULIRG mergers, the open diamonds are shell ellipticals, and the triangle is NGC 5812, the elliptical galaxy common to both this study and P98. NGC 1614 and NGC 2623, the two LIRGs with Ca triplet and CO velocity dispersions are plotted twice. The Ca triplet and CO derived data points are connected by a solid line to make a comparison easier. The five-point stars are the data points for NGC 1614 and NGC 2623 using the CO velocity dispersion. The “x” symbols in the plot are ellipticals from P99 which were used to derive the Fundamental Plane in P98. While P98 used early-type galaxies, including S0’s and some peculiar E’s, to construct the fundamental plane, only galaxies classified as “pure” ellipticals are plotted from the P99 sample. They are plotted in addition to the best-fit line in order to show the scatter present among the ellipticals and to compare that with the scatter among the mergers.

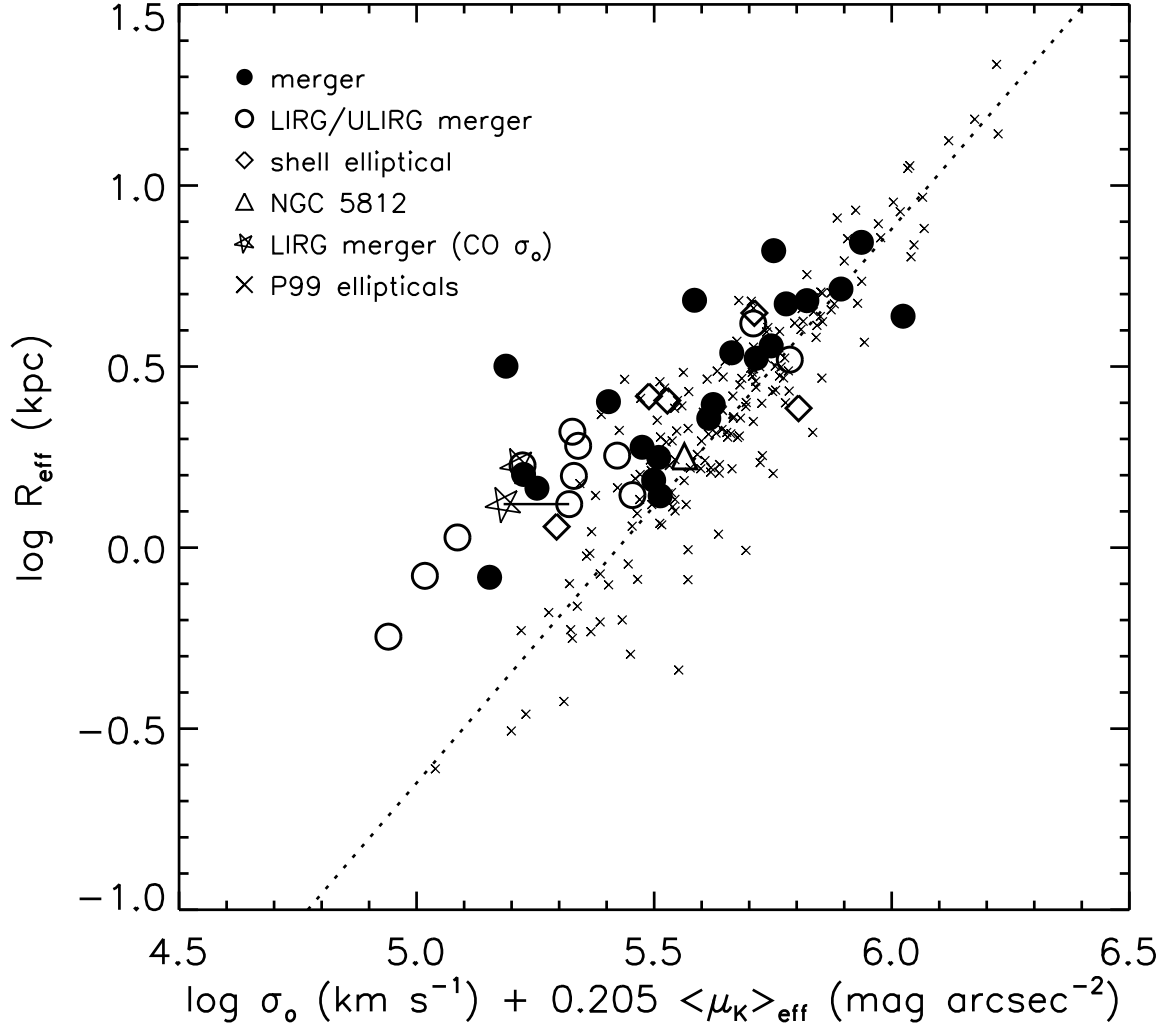


Fig. 1.— The  $K$ -band Fundamental Plane of Elliptical Galaxies from P98. The dotted line is the Fundamental Plane,  $\log R_{\text{eff}} = 1.53 \log \sigma_0 + 0.314 \langle \mu_K \rangle_{\text{eff}} - 8.30$ . The filled circles are normal mergers, the open circles are the LIRG/ULIRG mergers, the open diamonds are the shell ellipticals, and the five-point stars are the LIRGs NGC 1614 and NGC 2623 plotted using the CO derived  $\sigma_0$ . Their points are connected by a solid line to the Ca triplet derived values to make a comparison easier. The open triangle is the “control” sample elliptical, NGC 5812. The Spearman Rank coefficient indicates that the mergers show a strong correlation between the Fundamental Plane parameters at a significance of 0.001. The slope of the mergers on the Fundamental Plane is 0.84 with a scatter of 0.135 dex.

In general, a majority of the mergers appear to lie on the Fundamental Plane or within the same scatter of the ellipticals from P99. The mergers show evidence of a strong correlation among the parameters of the Fundamental Plane. The Spearman Rank Correlation was used to test this statistically. This test was selected because it is non-parametric, it makes no assumption about the shape of the distribution. The only assumption made is that the distribution is continuous. The Spearman Rank Correlation coefficient indicates a strong correlation of the parameters at significance level of 0.001. The scatter of the mergers is only 0.135 dex, compared with 0.096 dex for the ellipticals from P98. However, the slope of the merger line is 0.84, which differs from the slope of 1.53 for the  $K$ -band Fundamental Plane. Visually, the mergers in Figure 1 appear to show evidence of a “tail”-like feature at values of smaller  $R_{\text{eff}}$ , brighter  $\langle\mu_K\rangle_{\text{eff}}$  and smaller  $\sigma_{\circ}$ . Somewhere around 20% of the mergers appear to lie within this offset region. No mergers appear to lie beyond the scatter of the P99 ellipticals to the right of the Fundamental Plane. If the offset of mergers from the Fundamental Plane were due purely to random scatter and/or a poor correlation among the parameters, then there should be no preferred direction or structure. Two possible explanations for the offset are an evolutionary difference, suggesting these objects will eventually reach the Fundamental Plane, or these mergers are somehow physically different, and may never reach the Fundamental Plane. Michard & Prugniel (2004) conducted a study of peculiar ellipticals taken from a catalog of early-type galaxies (Prugniel & Simien 1996). They found the peculiar ellipticals systematically deviated from both the Fundamental Plane and Faber-Jackson relation. The primary reason for the deviation is the presence of a younger population of stars. The peculiar ellipticals were found to be brighter than expected and have smaller  $\text{Mg}_2$  indices as compared with non-peculiar or “normal” ellipticals.

While photometric properties such as  $R_{\text{eff}}$  and  $\langle\mu_K\rangle_{\text{eff}}$  can change over time as a result of star-formation and stellar evolution, the central velocity dispersion does not. Merger simulations, i.e. (Barnes 1988, 1992), suggest that once a single nucleus is formed the central velocity dispersion becomes fixed. All the mergers in the sample were selected based on the presence of single nucleus, therefore, their observed  $\sigma_{\circ}$  is unlikely to change. The mergers offset from the Fundamental Plane lie in a region where a lower  $\sigma_{\circ}$  *may* contribute partially or solely to the difference. Therefore, it is important to test whether the dispersions of the mergers are consistent with elliptical galaxies. If they are, then the offset is the result of photometric differences which can change over time.

### 5.1.1. Kinematic versus Photometric Differences

Figure 2 shows a rotated view of the Fundamental Plane, with the photometric and kinematic observables separated. The symbols and overplotted dotted line are the same as Figure 1. This projection of the Fundamental Plane shows the offset is more the result of photometric differences than kinematic ones. Only one merger, NGC 4004, lies outside of the range of the P99 central velocity dispersions. Furthermore, the mergers appears to be skewed towards larger values of  $\sigma_{\circ}$  relative to the P99 sample.

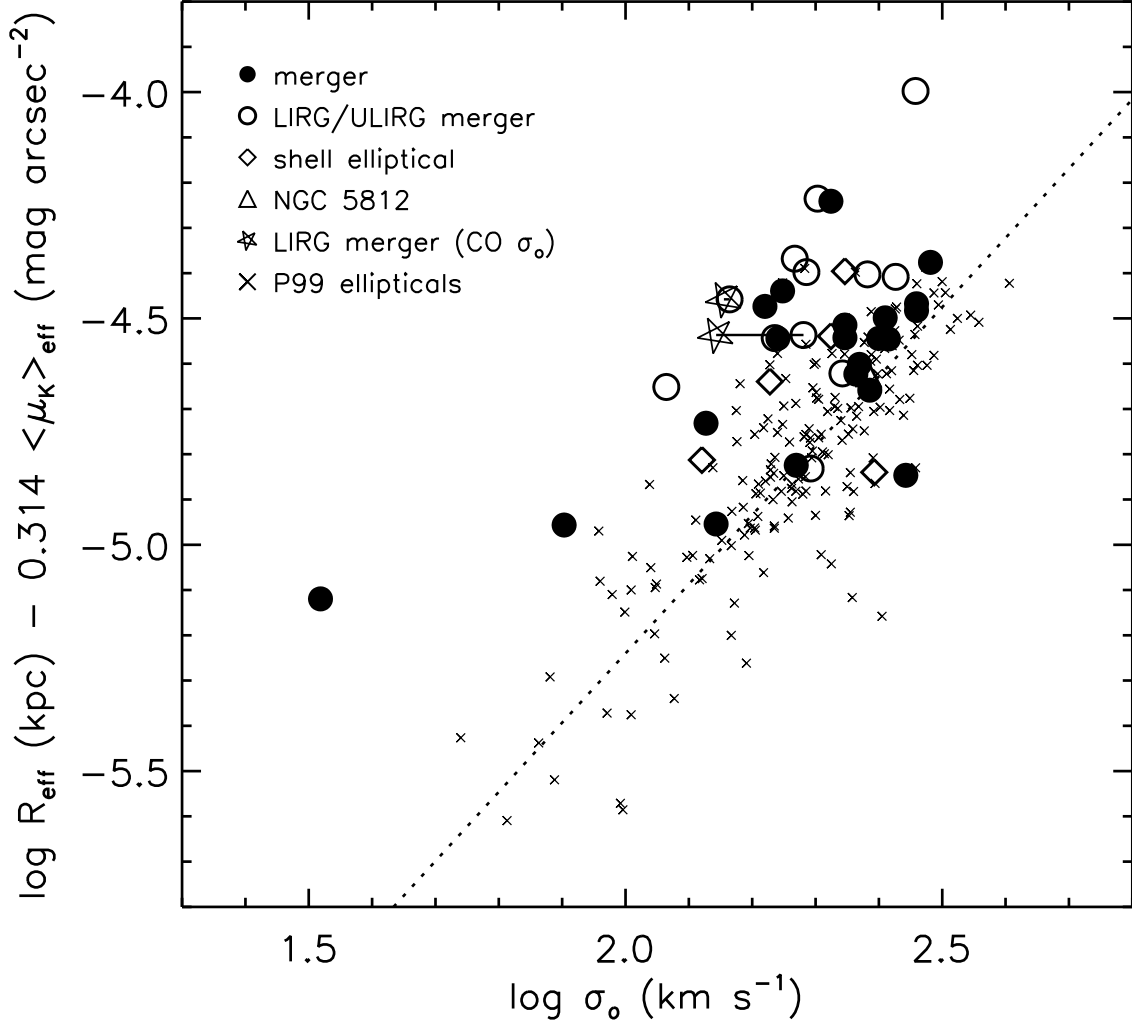


Fig. 2.— Figure 2 shows the Fundamental Plane projected so that the photometrically and kinematically observed properties are separated. The symbols and dotted line are otherwise the same as Figure 1.

A more quantitative analysis was conducted using a Kolmogorov-Smirnov (K-S) two-tailed test to compare the mergers and each sub-sample with other galaxy samples. The K-S test probes the null hypothesis that two distributions in question arise from the same parent population. It is a non-parametric test, it makes no assumptions about the form of the parent distribution. The only assumption is that the two distributions are continuous. A K-S test comparing the  $\sigma_o$  of the merger sample and the P99 sample of elliptical galaxies shows the null hypothesis cannot be rejected. That is, they appear to arise from the same parent population. A comparison of the  $\log R_{\text{eff}}$  between the mergers and P99 ellipticals produces the same results. Finally, a comparison of the  $\langle \mu_K \rangle_{\text{eff}}$  between the mergers and P99 ellipticals rejects the null hypothesis at the 0.001 confidence level. These statistical results in conjunction with Figure 2 suggest that the difference in slope between the mergers and P99 ellipticals is more likely the result of photometric, not kinematic differences. The presence of a preferred direction in the offset of some mergers from the Fundamental Plane is also likely due to differences in the effective radius and higher surface brightness, rather than a low  $\sigma_o$ .

### 5.1.2. *Do Mergers form Massive Ellipticals?*

If mergers show a strong correlation among the Fundamental Plane parameters, an important question to ask is what type of elliptical they are likely to form. This question has been touched upon before in the literature. Schweizer (1982, 1996) points out that the optical luminosity of NGC 3921 and NGC 7252 are high enough to fall within the range of luminous giant ellipticals (gE’s). The results from Paper I suggest that most of the mergers, including LiRG and ULIRG types, are luminous enough at  $K$ -band to form ellipticals which are  $\geq L^*$ . However, Genzel et al. (2001) argue, based on the central velocity dispersions derived from the CO absorption line at 1.63 and 2.29  $\mu\text{m}$ , that ULIRG mergers will form only  $\sim L^*$  intermediate-mass ellipticals and cannot form gE’s. Citing the earlier CO studies of Shier & Fischer (1998) and James et al. (1999), they further suggest that LIRG mergers will form sub- $L^*$  intermediate-mass ellipticals. James et al. (1999) note for their sample that a K-S test shows that the central velocity dispersions of their merger sample are consistent with *both* spiral bulges and elliptical galaxies. These results are in stark contrast to predictions that LIRG/ULIRG mergers might be analogous to the objects which formed present-day gE’s at  $z > 1$  (Kormendy & Sanders 1992). One reason ULIRGs could be potential analogues to these objects for is the large quantities of molecular gas in these objects which provide enough fuel to trigger strong star-formation.

The kinematic data presented here provides an opportunity to test whether or not the luminosity and kinematics are both consistent with the suggestion that mergers can produce luminous giant ellipticals. Kinematic data were taken from the literature for samples of gE’s, intermediate-mass ellipticals, as well as spiral bulges, to test whether the kinematics and luminosities of the mergers produce consistent results or show the same disparities as earlier studies. A comparison with the bulges of spiral galaxies was also made because bulges are known to lie on the Fundamental Plane and possess stellar profiles similar to elliptical galaxies. The survival of a bulge during

a spiral-spiral merger could produce elliptical-like properties, including an  $r^{1/4}$  light profile within the inner several kpc. The sample of giant E’s and intermediate-mass ellipticals were taken from Bender et al. (1992) (hereafter BBF92). Only ellipticals designated as “pure-E”’s were used from BBF92. They divided their larger sample of ellipticals based on absolute luminosity and morphology: Giant elliptical were defined as  $M_B \leq -19.62$ , intermediate-mass ellipticals were defined as  $-19.62 < M_B \leq -17.62$  (for  $H_o = 75 \text{ km s}^{-1} \text{ Mpc}^{-1}$ ). In order to reduce possible errors introduced by the comparison of different aperture size, the  $\sigma_o$  of the ellipticals were corrected to the aperture diameter of 1.53 kpc used by P99.

The  $\sigma_o$  for 98 spiral bulges were taken from Whitmore, Schechter, & Kirshner (1979), Héraudeau & Simien (1998), Héraudeau et al. (1999), Falcón-Barroso, Peletier, & Balcells (2002) and Falcón-Barroso et al. (2003). No aperture corrections were applied to the  $\sigma_o$  of the bulges because it is not clear that  $\sigma_o$  changes with radius in the same fashion as elliptical galaxies. Aperture sizes were on average a few arcseconds in size. The sample selection was limited to spirals with  $cz \leq 4000 \text{ km s}^{-1}$  and  $M_B \leq -18$  (for  $H_o = 75 \text{ km s}^{-1} \text{ Mpc}^{-1}$ ). The late-type galaxies range from Sa through Scd.

The results indicate that the hypothesis that mergers and spiral bulges arise from the same parent population can be rejected at the 0.001 confidence level. The same results occur for each of the merger sub-samples, except the shell ellipticals. The hypothesis there can be rejected at the 0.05 confidence level. When the merger sample as a whole is compared with gE’s, the hypothesis that the two samples arise from the same parent population can be rejected at the 0.1 confidence level, which is rather weak. The hypothesis cannot be rejected for the merger sample as a whole when compared with the intermediate-mass ellipticals.

When the each of the merger sub-samples are compared separately with gE’s and intermediate-mass ellipticals, the results change somewhat. Table 8 shows the results of the K-S test for the mergers, merger sub-samples, as well as the LIRG/ULIRG mergers from the studies noted above, and mergers from Lake & Dressler (1986). They were all tested against gE’s, intermediate-mass ellipticals, and spiral bulges. The  $\sigma_o$  of the mergers from Lake & Dressler (1986) include those derived from both the Calcium triplet and Mg *I*b stellar absorption lines. The velocity dispersions derived from the Calcium triplet took precedence in the analysis, although the dispersions derived from both lines were similar. Figure 3 illustrates the results in histogram form. The bin size is  $25 \text{ km s}^{-1}$ . The data are plotted as a fraction of the total number for each sample.

Table 8. Confidence Levels for the Rejection of the Null Hypothesis that Two Samples Share the Same Parent Population

Sample	Giant Ellipticals Confidence Level	Intermediate-mass Ellipticals Confidence Level	Bulges Confidence Level
All Mergers	0.01	...	0.001
Normal Mergers	...	0.1	0.001
ULIRG/LIRG Mergers	0.1	...	0.001
Shell Ellipticals	...	...	0.05
Previous ULIRG/LIRGs studies	0.001	...	0.001
Mergers from Lake & Dressler	0.05	0.1	0.001

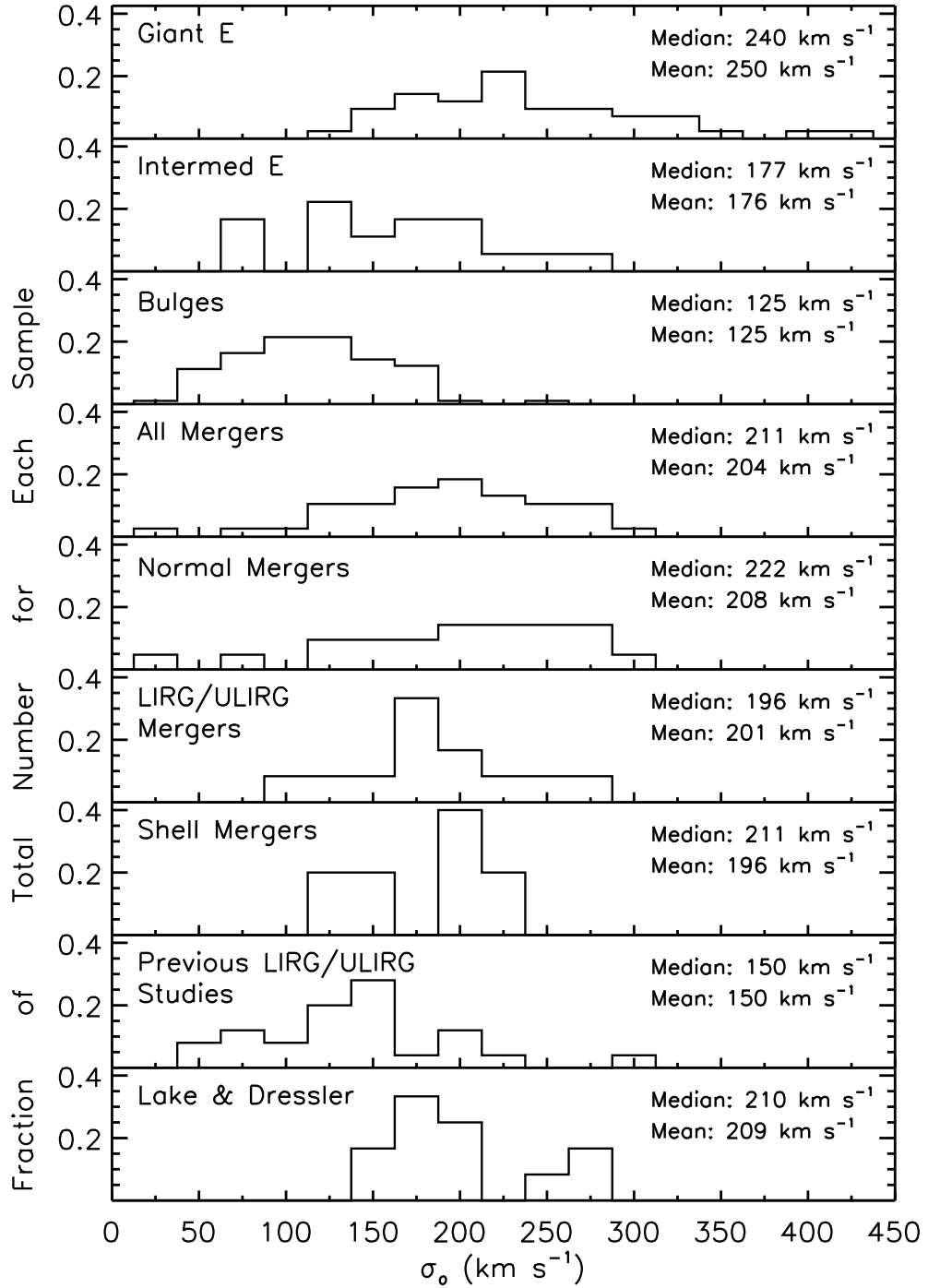


Fig. 3.— Figure 3 is a histogram which shows the distribution of the  $\sigma_0$  of the various merger samples compared with the gE's, intermediate-mass ellipticals, and spiral bulges. The bin size is  $25 \text{ km s}^{-1}$ . The data are plotted as a fraction of the total number for each sample. The median and mean  $\sigma_0$  of each sample are also listed.

The results in Table 8 and Figure 3 show that the  $\sigma_o$  of the normal mergers and shell ellipticals lie somewhere between intermediate-mass ellipticals and gE’s. The  $\sigma_o$  of the LIRG/ULIRG mergers are more akin to intermediate-mass ellipticals. However, the LIRG/ULIRG show larger  $\sigma_o$  than those in earlier studies. A K-S test between the earlier LIRG/ULIRG studies and the entire LIRG/ULIRG sub-sample in the current study indicates that at the 0.01 confidence level they do not share the same parent population. Yet six mergers from those earlier studies are part of the merger sample presented here.

This begs the question as to what differences exist between the studies which could produce different results. There are six mergers from the Lake & Dressler (1986) study that are also part of the merger sample presented in this paper. The same stellar absorption line was used in both studies to derive the central velocity dispersion. While the derived dispersions are not identical, the average difference between the Lake & Dressler study and this one is only  $\sim 6 \text{ km s}^{-1}$ . Two major differences between the previous LIRG/ULIRG studies and the current sample are the inclusion of objects with two distinct nuclei and the stellar absorption lines used to measure  $\sigma_o$ . The previous LIRG/ULIRG work cited used only the CO absorption line at either 1.63 or 2.29  $\mu\text{m}$ , whereas this study has relied primarily on the Ca triplet line at 8500 Å. A comparison of the  $\sigma_o$  derived from both the Ca triplet and CO lines for the objects common to both this and earlier studies show that in all but one case, the CO line is smaller by anywhere from a few percent to almost 50%. Figure 3 illustrates the differences in the distribution between the Ca triplet and CO derived dispersions for the LIRG/ULIRG mergers. Even for the two mergers in the present sample, NGC 1614 and NGC 2623, for which both Ca triplet and CO data were obtained using the same aperture size and the same telescope, there is a difference in the derived  $\sigma_o$ . This suggests that the Ca triplet and CO stellar absorption lines may not be probing the same stellar populations for some or possibly all of the mergers. These results may explain why earlier LIRG/ULIRG merger studies concluded that while many of these objects are as luminous as gE’s, their kinematic properties are quite different. The LIRG/ULIRG mergers in the present study indicate that they are not consistent with gE’s at only the 0.1 confidence level whereas earlier studies have shown this at the 0.001 confidence level. A more detailed discussion of the differences between the Ca triplet and CO  $\sigma_o$  is deferred to section 5.6

## 5.2. Mergers on the Fundamental Plane as seen in $\kappa$ -space

BBF92 developed a set of orthogonal transformations which allows the Fundamental Plane to be viewed directly in terms of mass and mass-to-light within the effective radius:

$$\kappa_1 \propto \log (M/k_2) \tag{5}$$

$$\kappa_2 \propto \log (k_1/k_2) (M/L) I_e^3 \tag{6}$$

$$\kappa_3 \propto \log (k_1/k_2) (M/L) \tag{7}$$

where  $k_1$ ,  $k_2$ , and  $k_3$  are structural constants and  $I_e$  is measured in units of  $L_\odot \text{ pc}^{-2}$  at  $K$ -band. The orthogonal transformations are not perfect. The  $\kappa$ -space transformation is a slightly tilted view of the Fundamental Plane. Thus, ellipticals on the Fundamental Plane show a slightly wider dispersion in their placement in  $\kappa$ -space.

Figure 4 shows the  $\kappa_1$ - $\kappa_3$  space for both the mergers and the P99 ellipticals. The symbols are the same as Figure 1.  $\kappa_1$  and  $\kappa_3$  are also given in quantities of the effective mass (in solar units) and effective  $M/L$  (in solar units). These conversions are derived from Appendix A of Burstein et al. (1997). The dotted line is the best-fit line from P98. The mergers show a strong correlation between  $\kappa_1$  and  $\kappa_3$ . The Spearman Rank Correlation Coefficient shows a strong correlation at confidence level of 0.001. The slope for the P99 ellipticals is 0.147 compared with 0.447 for the mergers. The mergers appear to have nearly the same overall distribution in effective mass as elliptical galaxies, but very different distributions of  $M/L$ . The presence of a “tail” noted earlier in the distribution of the mergers on the Fundamental Plane is illustrated in a more physical sense here, and is likely responsible for the steeper slope of the mergers. A K-S test comparing the  $(M/L)_{\text{eff}}$  ratio of the merger sample as a whole and the ellipticals shows that at a confidence level of 0.001 the two do not arise from the same parent population. The results are the same when comparing the normal and LIRG/ULIRG mergers with the P99 ellipticals. The confidence level is only 0.1 between the shell ellipticals and P99 ellipticals. Ellipticals have a much higher  $(M/L)_{\text{eff}}$  ratio for the same given mass.

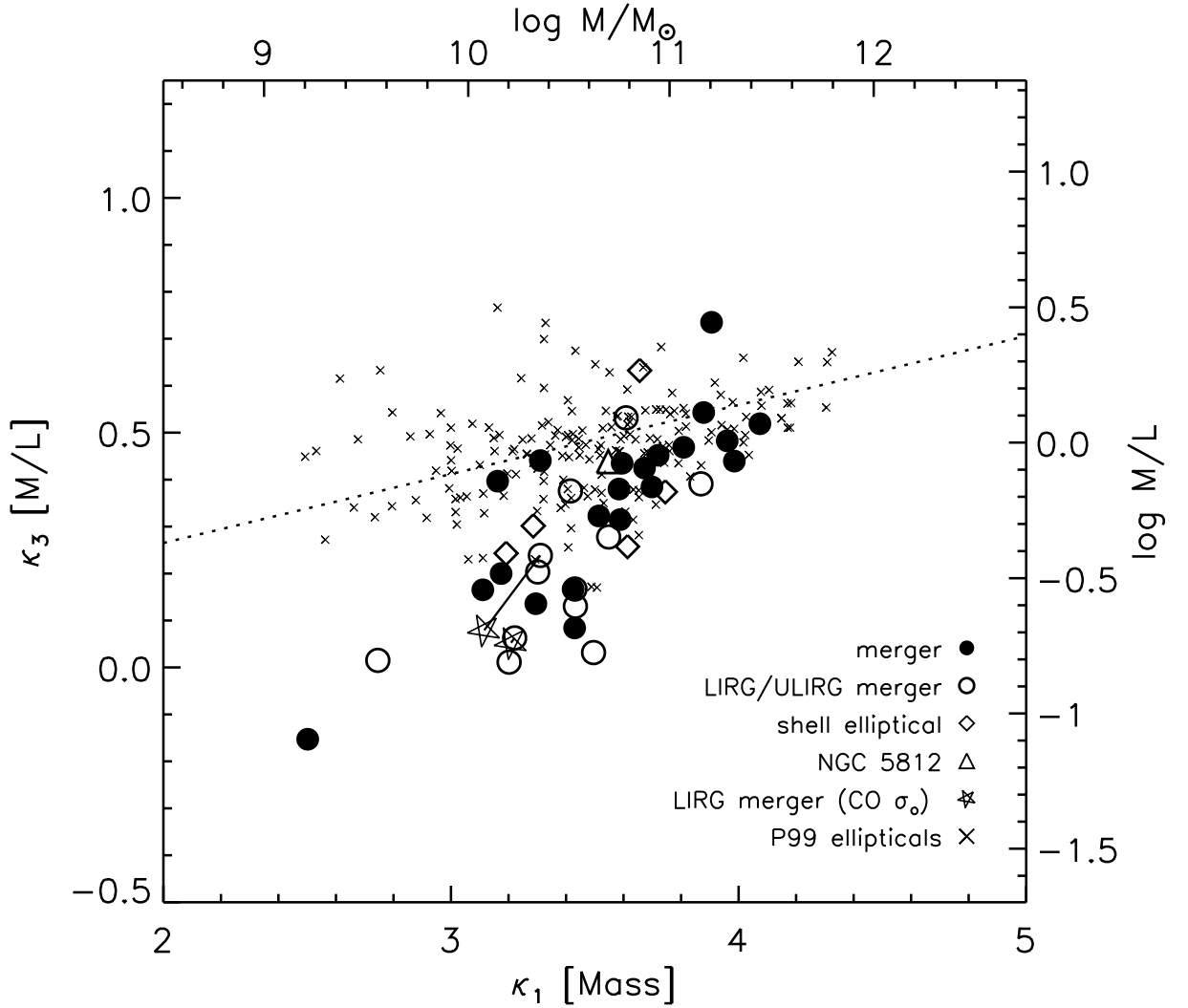


Fig. 4.—  $\kappa$ -space projection of the Fundamental Plane as first formulated by BBF92. The axes are orthogonal transformation of the more familiar Fundamental Plane parameters such that  $\kappa_1 \propto \log M/M_\odot$  and  $\kappa_3 \propto M/L_{\text{eff}}$ . The symbols are the same as in Figure 1. The dotted line is the best-fit to the early-type galaxies from P98. The merger samples shows an obvious difference in the  $M/L_{\text{eff}}$  ratio as compared with the P99 ellipticals.

The scatter of some mergers off of the Fundamental Plane has been shown to be the result of photometric differences. This result is borne out in the  $\kappa$ -space projection as well. The differences in the the  $(M/L)_{\text{eff}}$  ratios at a given mass may be evidence of strong star-formation occurring in the mergers. Zepf & Silk (1996) modeled the changes in the scaling of  $M/L$  versus  $M$  for elliptical galaxies. They found that the slope for elliptical galaxies may be explained by a burst of star-formation. The “tail”-like structure in both the Fundamental Plane and  $\kappa_1$ - $\kappa_3$  diagrams is dominated by the LIRG/ULIRG galaxies, which are known to contain vast quantities of molecular gas. These objects are also known to produce super-starbursts. Mouhcine & Lançon (2003) modeled the photometric evolution of single stellar populations from 50 Myr to 15 Gyr over a range of metallicities. One of the goals was to model the evolution of the stellar mass-to-light ratio in the  $V$ -band and  $K$ -band. The models followed the zero age main sequence (ZAMS) to the thermally pulsing regime of the asymptotic giant branch phase (TP-AGB). The results showed as the population evolved, the  $K$ -band  $M/L$  increased. However, a flattening did occur in the evolution of  $M/L$  only at  $K$ -band as a result of the presence of TP-AGB stars. Thus, a younger stellar population should produce a smaller  $M/L$  ratio for mergers with similar mass to a given elliptical galaxy. As the central stellar population ages, the merger may move vertically towards higher values of  $(M/L)_{\text{eff}}$ . This suggests that the mergers which lie off of the Fundamental Plane may be undergoing a strong starburst which skews their true position on the Fundamental Plane. Kinematically, they are consistent with elliptical galaxies, and as the starburst subsides then they may move towards the Fundamental Plane as their  $M/L$  ratios increase.

### 5.3. The Kormendy Relation

As noted earlier, differences in the surface brightness and effective radius appear to be responsible for any offsets between the mergers and the Fundamental Plane (save for NGC 4004, which has a very small  $\sigma_o$ ). The rotated view of the Fundamental Plane and orthogonal transformation to  $M$  and  $M/L$  also appear to confirm this idea. There also exists a correlation between  $R_{\text{eff}}$  and  $\langle\mu_K\rangle_{\text{eff}}$ , first laid out by Kormendy (1977). This is essentially a photometric projection of the Fundamental Plane. Figure 5 is plot of this relation. The symbols are the same as in Figure 1. Unlike the previous figures, data for *all* 51 mergers in the sample are plotted because it does not require any kinematic information. A Spearman Rank Correlation indicates at the 0.001 confidence level that the mergers show a correlation between  $\log R_{\text{eff}}$  and  $\langle\mu_K\rangle_{\text{eff}}$ . The best-fit slope of the mergers is 0.126 compared with 0.244 for the P99 ellipticals. The range in  $\langle\mu_K\rangle_{\text{eff}}$  is much broader than the P99 ellipticals, extending from 19.25 mag arcsec<sup>-2</sup> to 10.68 mag arcsec<sup>-2</sup>. However, the range in  $\log R_{\text{eff}}$  is much more limited. Unlike  $\langle\mu_K\rangle_{\text{eff}}$ , there is no scatter in  $R_{\text{eff}}$  beyond that of the P99 ellipticals. Overall, the mergers seem to show a scatter towards higher  $\langle\mu_K\rangle_{\text{eff}}$  than the P99 ellipticals. Furthermore, nearly all of the LIRG/ULIRG mergers lie to the right of the relation, indicating their  $\langle\mu_K\rangle_{\text{eff}}$  are much higher than the other two sub-samples.

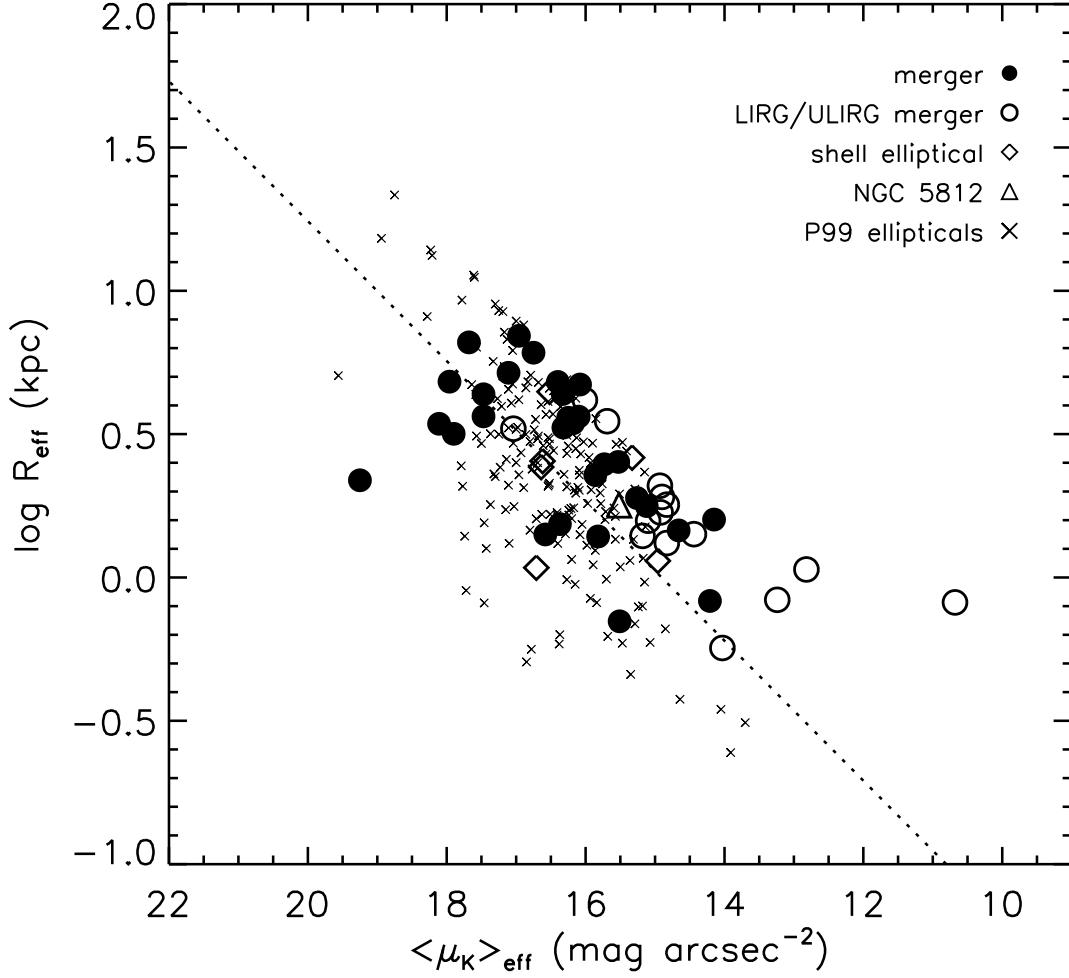


Fig. 5.— The  $K$ -band “Kormendy Relation” between  $\log R_{\text{eff}}$  and  $\langle \mu_K \rangle_{\text{eff}}$ . The symbols are the same as Figure 1. The dotted line is the best-fit to the early-type galaxies from P98. A Spearman Rank Correlation indicates at the 0.001 confidence level that the mergers show a strong correlation between  $\log R_{\text{eff}}$  and  $\langle \mu_K \rangle_{\text{eff}}$ .

#### 5.4. The $\text{Mg}_2$ - $\sigma_o$ Relation

The correlation between  $\text{Mg}_2$  and  $\sigma_o$  has implications regarding both the age and metallicity of elliptical galaxies. It has been known for some time that  $\text{Mg}_2$  shows a correlation with  $\sigma_o$  (Tonry & Davis 1981; Terlevich et al. 1981). Elliptical galaxies with larger velocity dispersions show stronger  $\text{Mg}_2$  strength. This correlation is important to investigate because the evidence so far indicates that differences in stellar populations and age may account for the photometric differences between mergers and elliptical galaxies. This is the first time that a large sample of mergers has been tested to determine whether they show the same correlation between  $\text{Mg}_2$  and  $\sigma_o$ . Table 7 lists the  $\text{Mg}_2$  magnitudes for each merger. Figure 6 shows the  $\text{Mg}_2$ - $\sigma$  correlation. The dotted line is the best-fit to the Pahre elliptical sample from P98. The mergers do not show the same correlation. A K-S test shows at the 0.001 confidence level that the P99 sample of ellipticals and mergers do not arise from the same parent population. The Spearman Rank Correlation Coefficient indicates that mergers show a correlation between  $\text{Mg}_2$  and  $\sigma_o$  at the 0.01 significance level. The figure shows nearly a bi-model distribution of the sample between those with negligible values of  $\text{Mg}_2$  and those approaching similar values to elliptical galaxies. Moreover, *all* of the LIRG/ULIRG mergers lie far from the best-fit elliptical relation.

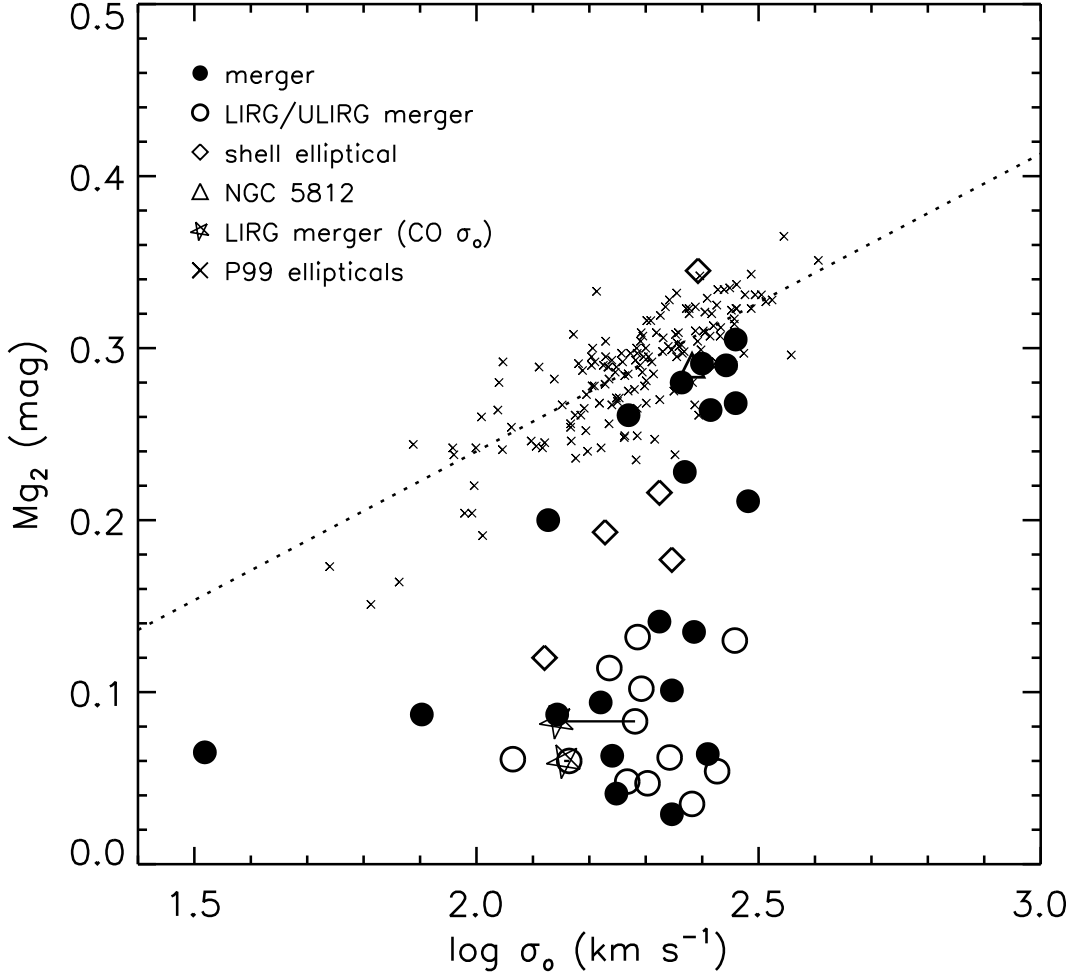


Fig. 6.— The  $Mg_2$ - $\sigma_0$  correlation for elliptical galaxies. The symbols are the same as Figure 1. The dotted line is the best-fit to the early type galaxies in P98. The mergers show a very large scatter, and no correlation between the parameters. The Spearman Rank Correlation Coefficient indicates that mergers show a correlation between  $Mg_2$  and  $\sigma_0$  at the 0.01 significance level.

The lack of a strong correlation for mergers between mass and metallicity at first appears to be at odds with the strong correlations shown for the Fundamental Plane and Kormendy Relation, as well as their kinematic similarities to elliptical galaxies. However, the presence of strong star-formation may dilute the  $Mg_2$  absorption line. de Carvalho & Djorgovski (1992) found that field ellipticals showed a larger scatter than cluster ellipticals in parameter correlations sensitive to stellar population differences, such as the  $Mg_2$  index. Forbes, Ponman, & Brown (1998) showed that the scatter in the  $Mg_2$  index is affected by the presence of a young burst population using instantaneous burst models from Bruzual & Charlot (1993). Strong emission lines, in particular from nearby  $H\beta$  and [O III] lines can affect the shape and depth of the  $Mg_2$  line. Continuum emission from young stars can also fill in the Mg lines, producing a smaller index.

A similar conclusion was reached by Michard & Prugniel (2004) in their study of peculiar ellipticals. They found that most of the peculiar ellipticals in their sample had smaller than expected  $Mg_2$  indices. These objects were found to have optical colors and spectral line indices consistent with the presence of a younger stellar population. However, their results also showed that  $\sim$  one-third of the peculiars have normal or even reddish stellar populations. They concluded that this is likely the result of either interactions between old galaxies with ISM’s insufficient to produce new stars or a mixture of medium age and high metallicity stars. Overall, the more extreme the peculiarity, the more likely that the population is younger. This does appear to fit within the paradigm for mergers-make-ellipticals. As the newly formed ellipticals lose their “scars” from the merger, the stellar populations become more consistent with typical elliptical galaxies and the scatter from the Fundamental Plane decreases. Figure 7 is a plot of the  $Mg_2$  index plotted against the  $K$ -Band Fundamental Plane residuals ( $\Delta FP = \log R_{\text{eff}} - 1.53 \log \sigma_{\circ} + 0.314 \langle \mu_K \rangle_{\text{eff}} - 8.30$ ). Overplotted are the P99 ellipticals. A Spearman Rank Correlation Coefficient indicates at the 0.001 confidence level that  $\Delta FP$  is anti-correlated with  $Mg_2$ . The P99 ellipticals show a much weaker correlation at the 0.05 confidence level. Jorgensen, Franx, & Kjaergaard (1996) found a similar weak correlation at optical wavelengths, however, they attributed it to a “left-over” correlation with  $\sigma_{\circ}$ . In the case of the mergers, the correlation between  $Mg_2$  and  $\sigma_{\circ}$  is significantly weaker than the correlation between  $\Delta FP$  and  $Mg_2$ . Thus, it is possible that the correlation in Figure 7 shows that any offset of the mergers from the Fundamental Plane is the result of differences in the stellar population with elliptical galaxies. A more detailed treatment of the stellar populations of the merger sample using diagnostics such as the Lick Indices and population synthesis models should be able to confirm or reject this possibility.

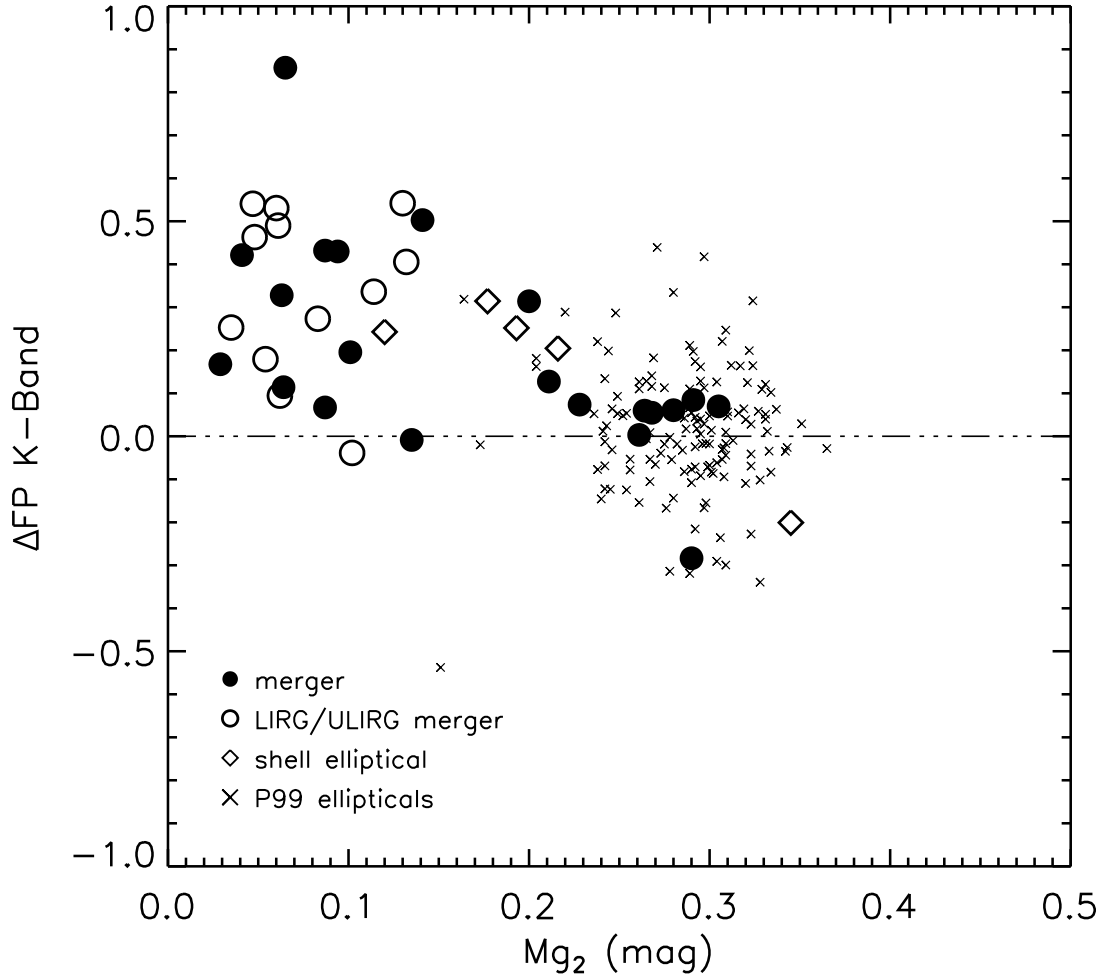


Fig. 7.— Comparison of the  $K$ -Band FP residuals with  $Mg_2$ . The symbols are the same as Figure 1. The Spearman Rank Correlation Coefficient indicates that mergers show a strong anti-correlation (at the 0.001 confidence) between their distance from the Fundamental Plane and the  $Mg_2$  index. The smaller the index, the more offset from the Fundamental Plane. The P99 ellipticals show a very weak correlation at the 0.05 confidence level.

### 5.5. The Phase-Space Density of Mergers

A serious criticism of the merger picture which emerged early on is the discrepancy between the central densities of disk galaxies and ellipticals. Merging two stellar disks cannot bring the central phase-space density to the same levels observed in most elliptical galaxies (Gunn 1987). Carlberg (1986) showed that phase-space densities increase as  $L$  decreases ( $f_c \propto L^{-2.35}$ ). Using a cooling diagram, Kormendy (1989) showed that the amount of dissipation needed to produce ellipticals increases as the luminosity decreases. Only high-luminosity disks can form the the brightest elliptical galaxies. Kormendy & Sanders (1992) suggested that ULIRG mergers can overcome this problem. Observations have shown that for some of these objects the mass in gas is equal to the mass in stars in the central kpc (Scoville et al. 1991; Sargent & Scoville 1991) and are more centrally concentrated than in spiral galaxies (Casoli et al. 1991). This would suggest a strong dissipation of gas to the central region of the merger which can trigger a starburst (Barnes & Hernquist 1991; Mihos & Hernquist 1994). Even non LIRG/ULIRG mergers are known to contain large quantities of gas (Dupraz et al. 1990; Hibbard & van Gorkom 1996). It has been shown observationally that most mergers undergo strong star-formation (Schweizer 1987; Joseph & Wright 1985). While numerical models predict that a starburst triggered by gaseous dissipation should increase the phase-space densities of mergers, the observational evidence to support this has been lacking.

Figure 8 shows a plot of the effective phase-space density ( $f_{\text{eff}}$ ) for the mergers and the P99 sample of elliptical galaxies. In addition, the bulges of spiral galaxies are also plotted to compare with the mergers. The data for the spiral bulges come from Möllenhoff & Heidt (2001) and Falcón-Barroso et al. (2002). The data from Falcón-Barroso et al. (2002) did not include  $M_K$  for the bulges.  $M_K$  for the bulges was derived by first taking  $M_R$  from Falcón-Barroso et al. (2003) and then using the  $(R-K)$  colors of each of the bulges from Peletier & Balcells (1997) to convert  $M_R$  to  $M_K$ . The dotted box labeled “Spirals” approximates the position of late-type disk galaxies in the  $f_{\text{eff}}-M_K$  plane. The values for late-type galaxies were taken from Mao & Mo (1998) and converted from  $B$ -band to  $K$ -band using  $(B-K)$  colors from Girardi et al. (2003). In addition to simple color conversion, the scale length and vertical scale height used by Mao & Mo (both of which are factors in approximating an effective radius for late-type galaxies) must be adjusted from  $B$ -band to  $K$ -band because they are larger at  $B$ -band by a factor of  $\sim 1.2-2\times$  (Peletier et al. 1994). All data has been corrected to  $H_o = 75 \text{ km s}^{-1} \text{ Mpc}^{-1}$ .

The parameter  $f_{\text{eff}}$  was defined by Hernquist et al. (1993) as way of estimating the phase-space density from observed parameters:

$$f_{\text{eff}} \equiv \left[ \frac{1}{\sigma_o R_o^2} \right] \quad (8)$$

It is similar to the phase-space density used by Carlberg (1986) except it replaces  $r_c$  from a King profile with  $r_{\text{eff}}$ , the half-light radius derived from a de Vaucouleurs  $r^{1/4}$  fit to the surface brightness profile. The results in Figure 8 show that phase-space densities of the mergers are very close to those of elliptical galaxies. This suggests that the mergers have undergone dissipative collapse.

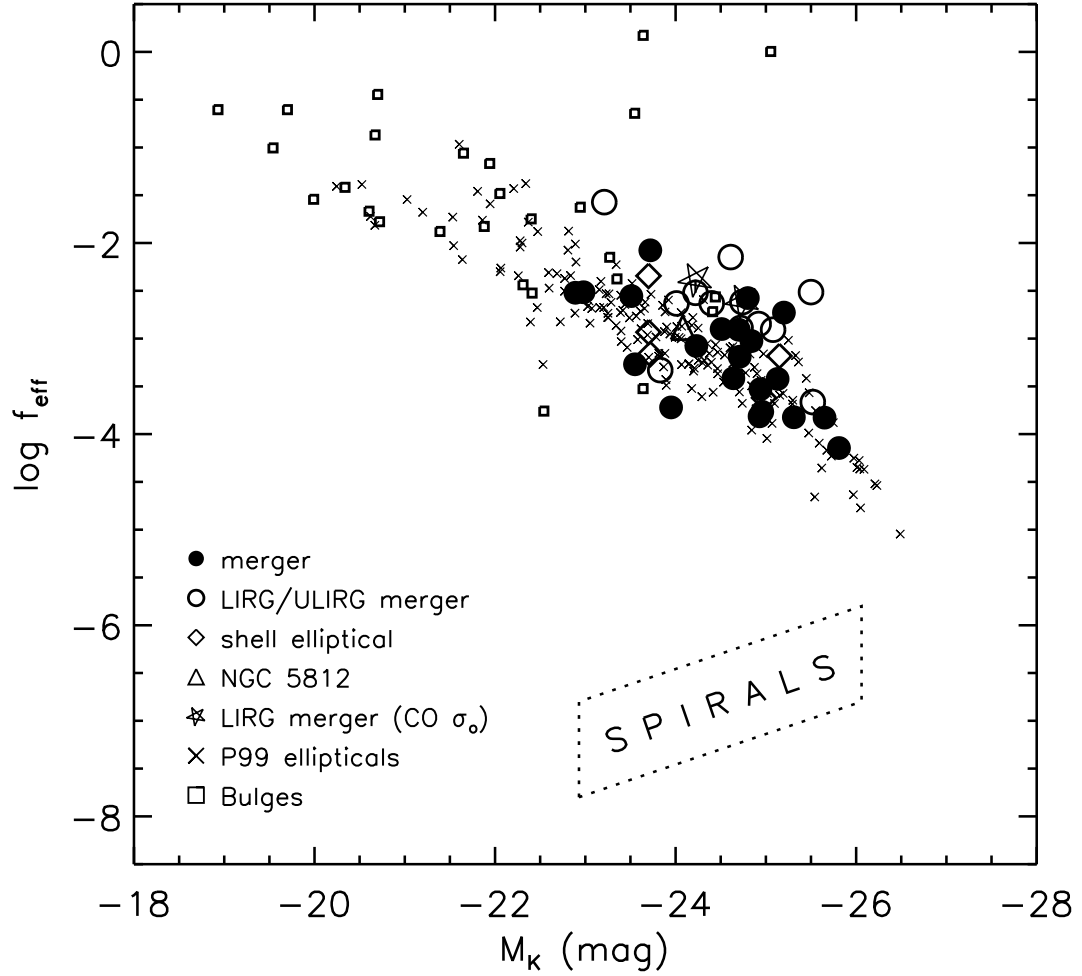


Fig. 8.— Plot of the effective phase-space ( $f_{\text{eff}}$ ) defined by Hernquist et al. (1993). The symbols are the same as Figure 1, however, they also include a sample of bulges (squares) as a comparison. In general, the  $f_{\text{eff}}$  of the merger sample is consistent with elliptical galaxies. The LIRG/ULIRG mergers do have a higher  $f_{\text{eff}}$  than the other mergers in the sample.

A K-S test comparing the  $f_{\text{eff}}$  of the mergers with the P99 ellipticals indicates that two populations likely share the same parent population. The same results are found when the normal merger and shell elliptical sub-samples are compared with the P99 ellipticals. However, the null hypothesis is rejected at the 0.1 confidence level between the LIRG/ULIRG mergers and P99 ellipticals. The LIRG/ULIRGs in Figure 8 have a higher phase-space density compared with the normal mergers, shell ellipticals, and P99 ellipticals.

### 5.6. Comparison of Ca triplet and CO velocity dispersions

As noted in Section 5.1, there are significant differences between the velocity dispersions derived from the Ca triplet at  $\sim 8500 \text{ \AA}$  and the CO line at  $2.29 \mu\text{m}$ . These differences have led to different conclusions on the end-state of mergers, in particular, LIRG/ULIRG mergers. Even within this study here, one of the two mergers with both Ca triplet and CO measurements shows significant differences in the derived  $\sigma_{\circ}$ . Discrepancies in data reduction and analysis between the Ca triplet and CO absorptions lines can be ruled out. The galaxies were measured using the same 1.53 kpc aperture size in the spatial direction, as well as with identical position angles. The slit width used for the Ca triplet line was  $0''.5$  and was  $0''.432$  for the CO line. Both the Ca triplet and CO lines were fit in exactly the same manner, using a Gauss-Hermite polynomial fit in pixel-space to determine the LOSVD. The continuum were normalized in a similar fashion. The only difference in the fitting routine were the template stars used. The best fit template star using the Ca triplet line for NGC 1614 was a G0III star, HD 332389 and for NGC 2623 a G8III star, HD 100347. In the near-infrared, the best fit template star for NGC 1614 was an M7.5III, Rx Boo and for NGC 2623 an M0III star,  $\lambda$  Dra. M-giant template stars were tested with the Ca triplet lines for NGC 1614 and NGC 2623 and found to be 2-3 times poorer fits than the G-type giants. The earliest CO template star observed was a K0III. However, the depth of the CO line in the K0III star was found to be too shallow as compared with the depth of the CO line for both NGC 1614 and NGC 2623.

Table 9 lists mergers in the present sample for which CO derived  $\sigma_{\circ}$  also exist in the literature. Only 1 merger, Arp 193, has a larger CO derived  $\sigma_{\circ}$ . A K-S test between the Ca triplet and CO derived dispersions rejects at the 0.025 confidence level that the two populations arise from the same parent population, even though the mergers are identical.

Table 9. Comparison of Ca triplet and CO derived  $\sigma_0$ .

Merger Name	Ca Triplet $\sigma_0$ km s <sup>-1</sup>	CO $\sigma_0$ km s <sup>-1</sup>
NGC 1614	146	143, <sup>1</sup> 75 <sup>2</sup> , 154 <sup>4</sup>
NGC 2623	191	139, <sup>1</sup> 95 <sup>3</sup>
NGC 3256	241	113 <sup>4</sup>
NGC 4194	116	104 <sup>5</sup>
Arp 193	172	206 <sup>5</sup>
AM 2055-425	185	140 <sup>6</sup>
NGC 7252	166,177 <sup>7</sup>	123 <sup>5</sup>
IC 5298	193	151 <sup>3</sup>

Note. — (1) this study, (2) Shier et al. (1994), (3) Shier et al. (1996), (4) Oliva et al. (1995), (5) James et al. (1999), (6) Genzel et al. (2001), (7) Lake & Dressler (1986)

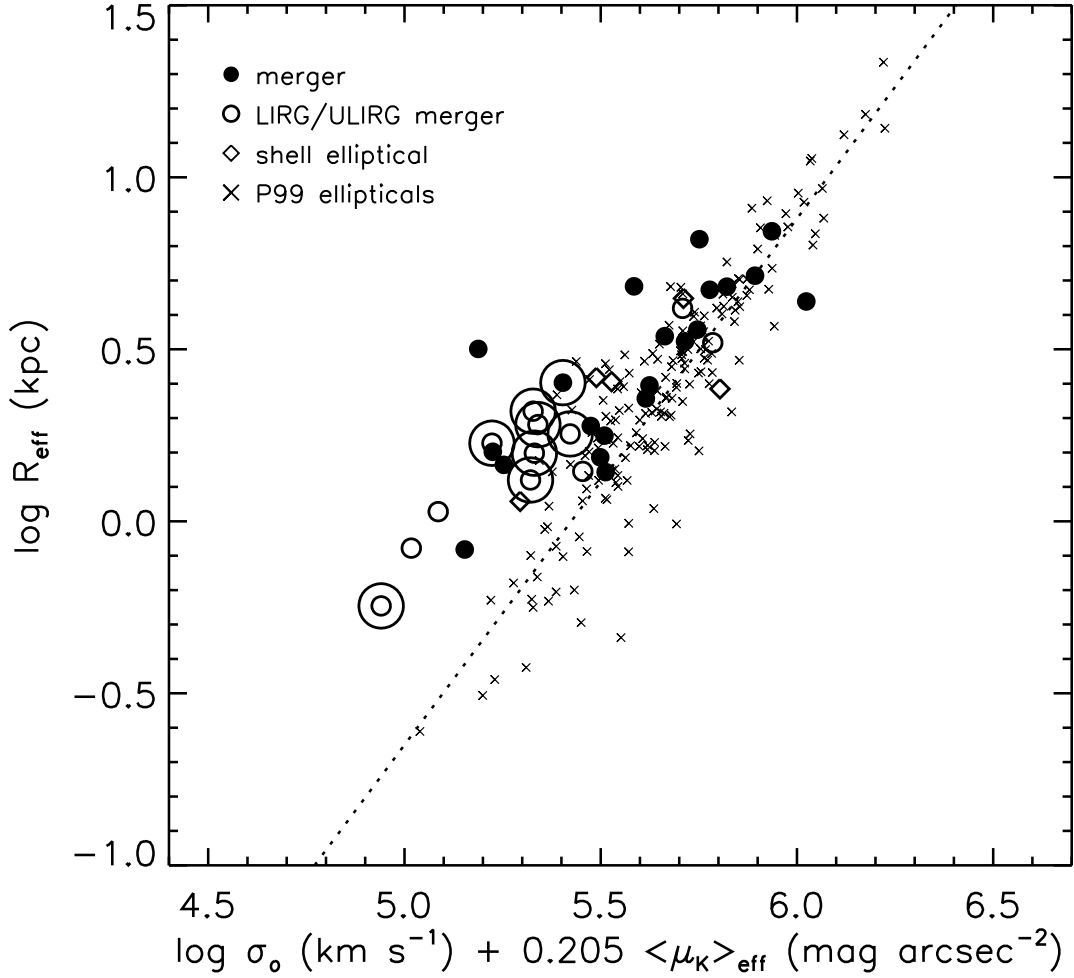


Fig. 9.— The  $K$ -band Fundamental Plane of Elliptical Galaxies as plotted in Figure 1 (symbols have the same meaning). The mergers in Table 9 are all circled to show where they lie on the Fundamental Plane. *ALL* of these mergers lie in the “tail” off of the FP.

These results raise questions about earlier merger studies which have relied solely on the CO absorption line to derive velocity dispersions. Are the stellar populations observed in the optical and infrared the same? However, before addressing that, it should be noted that *all* of the mergers in Table 9 lie in one specific region of the Fundamental Plane in Figure 1. Figure 9 shows the Fundamental Plane, plotted as it was in Figure 1, with the mergers that have both Ca triplet and CO dispersions circled. The plot shows the mergers with only the Ca triplet dispersions. The CO dispersions would shift the circled mergers further left (except for Arp 193). The circled mergers all lie within the “tail” noted earlier. If the CO velocity dispersions are used to plot the points, then all but one would shift further to the left.

If the mergers listed in Table 9 were distributed uniformly among the merger sample, then any conclusions drawn about the differences between the Ca triplet and CO absorption lines could be applied universally to all mergers, and, perhaps, even to some elliptical galaxies. However, the mergers in Table 9 may not be representative of all mergers. First, all but one are LIRG/ULIRGs. It has already been established that these mergers are somewhat different from “normal” mergers, in particular, they have a higher central surface brightness.

Silge & Gebhardt (2003) also found similar discrepancies for a sample of 25 early-type galaxies. They tested for systematic errors from continuum fitting and choice of template stars and found that at most they could account for  $\sim 5\text{-}10\%$  decrease in derived dispersions. Turning to a physical explanation, they compared  $Mg_2$  indices with CO equivalent widths and found no correlation. Furthermore, the equivalent widths of the CO lines were higher than expected from K-type giants and more in line with cool M-type giants. This suggests that the CO absorption line is not probing the same stellar population as the optical absorption lines. Oliva et al. (1999) point out that the CO 2.29  $\mu\text{m}$  band-head is primarily sensitive to micro-turbulent photospheric motions which increase at lower stellar temperatures and are larger in red supergiants (RSGs) than giants of a given temperature. In fact, they further point out that the CO line is essentially a degenerate diagnostic. Young stars of low metallicity and old, highly metallic cool red giants can have similar equivalent widths. Oliva et al. note difficulties in using equivalent widths to differentiate between stellar types. They *suggest* that an  $EW \geq 15 \text{ \AA}$  may be indicative of younger stars since that is larger than the EW of most metal-rich globular clusters. However, it is not uncommon to find some starbursts with a CO  $EW \leq 15 \text{ \AA}$ . The CO EWs of NGC 1614 and NGC 2623 are 14.4  $\text{\AA}$  and 12.7  $\text{\AA}$  respectively (using the EW definition from Origlia, Moorwood, & Oliva (1993)), which is close to the borderline, and consistent with either M-type giants or RSGs. Oliva et al. (1995) measured both the  $\sigma_o$  and the EW of NGC 3256 and derived a value of 12.9  $\text{\AA}$ . The Ca triplet EWs (using the CaT\* definition from Cenarro et al. (2001) ) are 5.1  $\text{\AA}$ , 6.3  $\text{\AA}$ , and 6.8  $\text{\AA}$  for NGC 1614, NGC 2623, and NGC 3256 respectively, which are more consistent with K or earlier giant stars.

This difference in which stellar population is probed depending on the optical or infrared absorption line used may be supported by the *K*-band photometry. As noted above, the mergers with both Ca triplet and CO observations lie are primarily all LIRG/ULIRGs which have much higher surface brightnesses compared with the other mergers in the sample. Mouhcine & Lançon (2002) modeled the contribution of asymptotic giant branch (AGB) stars to the total *K*-band

luminosity for a single-burst population. They found that the contribution evolves rapidly from a few percent at  $\simeq 0.1$  Gyr to  $\simeq 60\%$  of the light at 0.6-0.7 Gyr and then quickly declines soon after to  $\leq 30\%$ . The  $K$ -band light from these mergers may be dominated by AGB stars, which is what the CO absorption line is also detecting. The other mergers, which lie closer to, or on the plane, may be at a point where the light from AGB stars does not dominate the  $K$ -band continuum. It is unlikely that *all* of the mergers in the sample lie within the same narrow age range (0.1 Gyr) in which their light is dominated by contributions from AGB stars. Thus, it is possible that the CO  $\sigma_o$  may eventually match the Ca triplet line. A more detailed analysis of optical and infrared spectra of the nuclei should be able to determine whether these wavelength ranges are detecting the same stellar populations and constrain which mergers show strong contributions from AGB stars. Since ESI has a large optical wavelength range, the data used to derive velocity dispersions can also be used to get a handle on the stellar populations in the optical. Additional medium resolution ( $\lambda \sim 1200$ ) infrared spectra from 1-2.5 $\mu\text{m}$  have been obtained for  $\sim$  two-thirds of the sample using SPEX on the 3.0m IRTF and UIST on the 3.8m UKIRT. The optical and IR spectra have approximately the same slit width. These results will be presented in a subsequent paper. Additional high-resolution CO observations to derive  $\sigma_o$  for mergers which lie on the Fundamental Plane would be vital to determining whether the Ca triplet and CO derived dispersions will eventually match each other.

A second trend noted by Silge & Gebhardt (2003) was a decrease in the fractional differences in velocity dispersions when moving from S0 to E galaxies. This might be the result of dust which is both spatially coincident and geometrically aligned with a central disk. The dust would block the disk at optical wavelengths, yet be transparent in the infrared. Thus CO measurements would probe the motions of stars in the disk, producing smaller velocity dispersions. The presence of a central stellar disk in mergers is inferred from numerical models which predict the formation of a central gaseous disk as a result of gaseous dissipation (Barnes & Hernquist 1991; Barnes 2002). The  $K$ -band photometry from Paper I show a significant number of mergers have disk isophotes. This suggests that the Ca triplet and CO derived  $\sigma_o$  may never match each other. If this is the case, then it is important to consider which absorption line is a better measure of the dynamical mass of the system. If the CO absorption line is dominated by stars which lie in a central disk which produces smaller  $\sigma_o$ , then this disk may be de-coupled from the dynamics of the larger galactic system. Numerical simulations show that a central gaseous disk can form which could produce stars that are kinematically decoupled from the larger system. In other words, the central disk of stars would have been formed *in situ* and have no “knowledge” of the dynamics of the system as a whole. In contrast, the stars contributed from the progenitor spiral galaxies, would be sensitive to the dynamical state of the whole system.

## 6. Summary and Discussion

Below are a summary of the main results which have emerged from the data presented here:

1) Most of the mergers lie on or close to the Fundamental Plane (within the same scatter as the P99 ellipticals). Those mergers which lie beyond the scatter of the P99 ellipticals off of the

Fundamental Plane all fall within the same region and appear to form a discrete structure.

2) The  $\sigma_o$  of the mergers, with the exception of NGC 4004, are entirely consistent with those of elliptical galaxies. Furthermore, the dispersions appear to lie somewhere between values of intermediate-mass and giant elliptical galaxies. The  $\sigma_o$  of the LIRG/ULIRG mergers are larger than previous observations, placing them closer to giant ellipticals.

3) The differences between mergers which lie off of the Fundamental Plane and ellipticals appear to be solely photometric in nature.

4) Mergers show a very weak mass-metallicity correlation that is quite different from elliptical galaxies. Furthermore, the  $Mg_2$  index shows an anti-correlation with the residuals of the FP. The larger the  $\Delta FP$  the smaller the  $Mg_2$  index. This suggests that the differences between mergers and ellipticals may be due to differences in the stellar populations.

5) The central phase space density of mergers appear to be consistent with those of elliptical galaxies. This suggests that the mergers have undergone dissipation.

6) A significant difference has been found in the derived values of  $\sigma_o$  between the Ca triplet and CO absorption lines. The differences may be the result of the two absorption lines probing different stellar populations. A second possibility is that the CO line is probing a central dust enshrouded disk. The *only* way to confidently determine why a discrepancy exists is to obtain high-resolution CO observations of the mergers which lie on the Fundamental Plane.

The overall picture painted by these results suggests that spiral-spiral mergers produce objects which show nearly the same strong correlations between kinematic and photometric properties as elliptical galaxies (i.e. The Fundamental Plane). Any discrepancies between mergers and ellipticals have been shown not to be a function of  $\sigma_o$ . This is critical because the characteristic  $\sigma_o$  is likely to settle quickly to its final value after the two nuclei merge. This parameter will not evolve, or change over time. The major differences between mergers and ellipticals could be a function of the stellar populations. The evidence for this are the discrepancies in surface brightness,  $M/L$ , and metallicity. These suggest that a younger stellar population is superposed in the centers of the mergers, which increases their central luminosity and contaminates (i.e. “fills in”) or dominates the observed metallicities. The strong anti-correlation between  $\Delta FP$  and  $Mg_2$  strengthens this assertion. A possible secondary piece of evidence to support this is the discrepancies between the Ca triplet and CO derived  $\sigma_o$ . The CO absorption line is sensitive to both young, metal-poor RSGs as well as older late-type giants. If a strong starburst is present in the central regions of the mergers, the light from this could very well dominate the CO lines. These stars would be newly formed and would have no “memory” of the kinematics of the original late-type giants contributed from the two progenitors. This could explain why the  $\sigma_o$  are lower than those derived from the Ca triplet, which are probing the late-type giants. Furthermore, the phase-space densities of the mergers are consistent with those of elliptical galaxies. This supports the notion that these objects have undergone dissipative collapse, increasing the central stellar densities via a starburst to levels equivalent to elliptical galaxies. Cold or dissipationless merging can only form a giant elliptical galaxy from two massive spiral progenitors. If the mergers presented here were all the result of dissipationless merging, than their  $\sigma_o$  (both Ca triplet and CO) should *all* be consistent with the

most massive luminous elliptical galaxies ( $\sigma_o \gg 250 \text{ km s}^{-1}$ ).

The above conclusion is without a doubt painted in rather broad strokes and requires further analysis and observations to test its validity. First and foremost is to understand the nature of the Ca triplet and CO discrepancies. Unfortunately, all of the mergers which have CO measurements lie in an area offset from the Fundamental Plane. In order to constrain whether the discrepancy is the result of RSGs dominating the light, or a central stellar disk enshrouded in dust, CO observations are needed of mergers which lie *on* the Fundamental Plane. A more detailed analysis of the stellar populations using both optical and infrared absorption lines may help explain the lack of a strong mass-metallicity relationship as well as confirm that the offset of some mergers from the Fundamental Plane is the result of differences in  $M/L$  produced by younger stellar populations.

We would like to thank John Hibbard for helpful and informative discussions on earlier drafts of the paper, as well as Brad Whitmore and Roeland van der Marel for subsequent discussions which have improved the structure and content of the paper. A special thanks is given to Michael Cushing for his help and guidance on developing the IDL code used to measure the velocity dispersions from the extracted spectra. We would also like to thank Michael Connelley for taking  $K$ -band data of one of the mergers. This research has made use of the NASA/IPAC Extragalactic Database (NED) which is operated by the Jet Propulsion Laboratory, California Institute of Technology, under contract with the National Aeronautics and Space Administration. This research has been supported in part, by a Fellowship from the NASA Graduate Student Researchers Program, Grant # NGT5-50396.

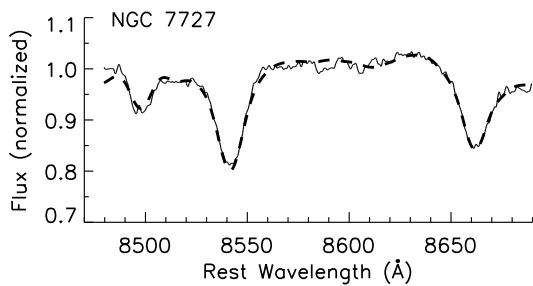
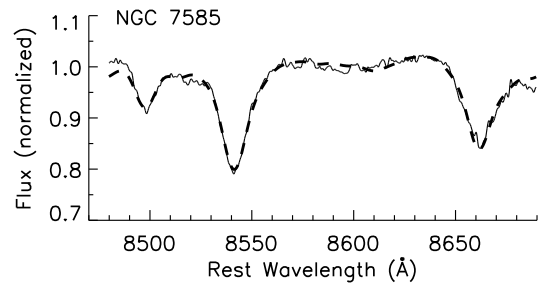
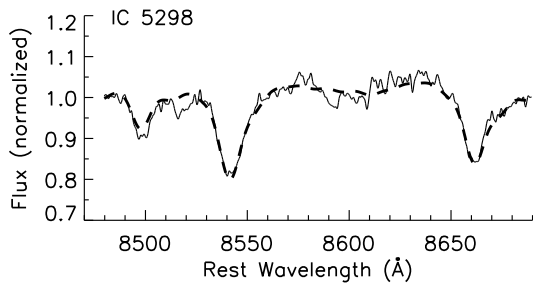
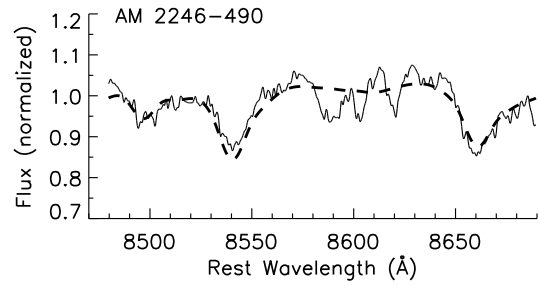
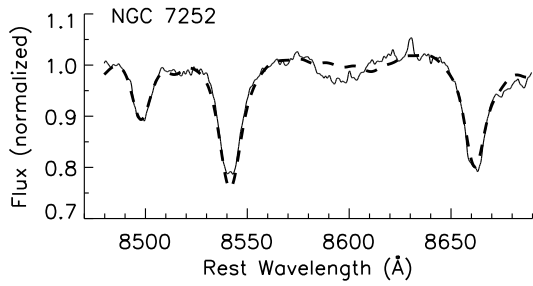
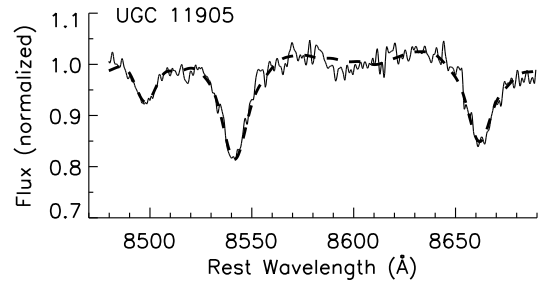
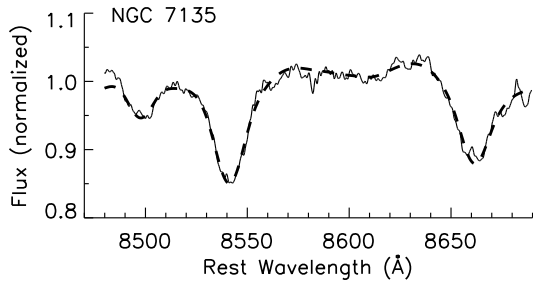
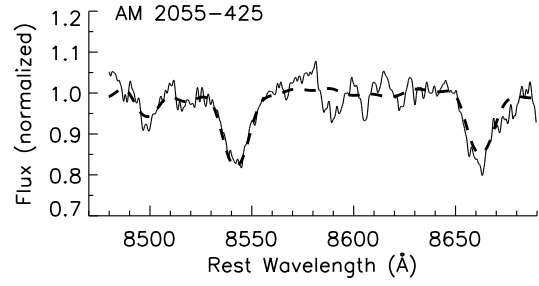
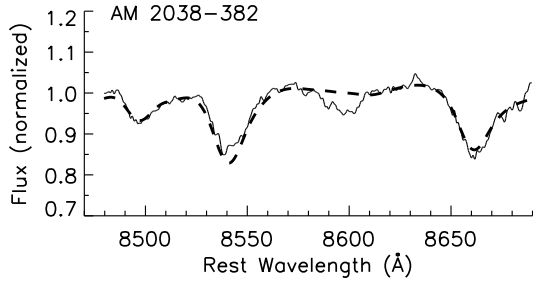
### A. Ca triplet and CO spectra

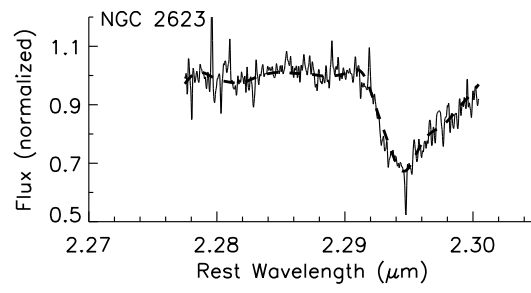
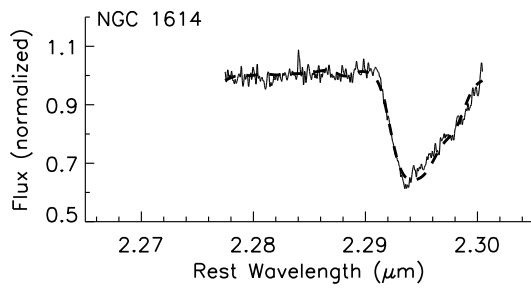
In this section we present the rest-frame wavelength spectra centered on the Calcium triplet absorption line for 38 mergers and 1 E0 galaxy in the sample, and the CO absorption line for 2 mergers in the sample. The solid line plotted in each figure is the galaxy spectrum, the superposed dashed-line is the convolved stellar template.











## REFERENCES

- Aaronson, M. 1981, in IAU Symp. 96: Infrared Astronomy, 297–314
- Arp, H. 1966, Atlas of Peculiar Galaxies (Publisher: California Institute of Technology, Pasaadena, CA, 1966)
- Arp, H. C. & Madore, B. F. 1987, A Catalog of Southern Peculiar Galaxies and Associations (Publisher: Cambridge University Press, 1987)
- Barnes, J. E. 1988, ApJ, 331, 699
- . 1992, ApJ, 393, 484
- . 2002, MNRAS, 333, 481
- Barnes, J. E. & Hernquist, L. E. 1991, ApJ, 370, L65
- Barth, A. J., Ho, L. C., & Sargent, W. L. W. 2002, AJ, 124, 2607
- Bender, R., Burstein, D., & Faber, S. M. 1992, ApJ, 399, 462
- Brodie, J. P. & Huchra, J. P. 1990, ApJ, 362, 503
- Bruzual, A. G. & Charlot, S. 1993, ApJ, 405, 538
- Burstein, D., Bender, R., Faber, S., & Nolthenius, R. 1997, AJ, 114, 1365
- Carlberg, R. G. 1986, ApJ, 310, 593
- Carter, B. S. & Meadows, V. S. 1995, MNRAS, 276, 734
- Casoli, F., Dupraz, C., Combes, F., & Kazes, I. 1991, A&A, 251, 1
- Cenarro, A. J., Cardiel, N., Gorgas, J., Peletier, R. F., Vazdekis, A., & Prada, F. 2001, MNRAS, 326, 959
- de Carvalho, R. R. & Djorgovski, S. 1992, ApJ, 389, L49
- Djorgovski, S. & Davis, M. 1987, ApJ, 313, 59
- Doyon, R., Wells, M., Wright, G. S., Joseph, R. D., Nadeau, D., & James, P. A. 1994, ApJ, 437, L23
- Dressler, A. 1984, ApJ, 286, 97
- Dupraz, C., Casoli, F., Combes, F., & Kazes, I. 1990, A&A, 228, L5
- Faber, S. M., Friel, E. D., Burstein, D., & Gaskell, C. M. 1985, ApJS, 57, 711

- Faber, S. M. & Jackson, R. E. 1976, *ApJ*, 204, 668
- Falcón-Barroso, J., Balcells, M., Peletier, R. F., & Vazdekis, A. 2003, *A&A*, 405, 455
- Falcón-Barroso, J., Peletier, R. F., & Balcells, M. 2002, *MNRAS*, 335, 741
- Forbes, D. A., Ponman, T. J., & Brown, R. J. N. 1998, *ApJ*, 508, L43
- Gaffney, N. I., Lester, D. F., & Doppmann, G. 1995, *PASP*, 107, 68
- Genzel, R., Tacconi, L. J., Rigopoulou, D., Lutz, D., & Tecza, M. 2001, *ApJ*, 563, 527
- Girardi, M., Mardirossian, F., Marinoni, C., Mezzetti, M., & Rigoni, E. 2003, *A&A*, 410, 461
- Gunn, J. E. 1987, in *Nearly Normal Galaxies. From the Planck Time to the Present*, p. 455
- Héraudeau, P. & Simien, F. 1998, *A&AS*, 133, 317
- Héraudeau, P., Simien, F., Maubon, G., & Prugniel, P. 1999, *A&AS*, 136, 509
- Hamuy, M., Suntzeff, N. B., Heathcote, S. R., Walker, A. R., Gigoux, P., & Phillips, M. M. 1994, *PASP*, 106, 566
- Hawarden, T. G., Leggett, S. K., Letawsky, M. B., Ballantyne, D. R., & Casali, M. M. 2001, *MNRAS*, 325, 563
- Hernquist, L., Spergel, D. N., & Heyl, J. S. 1993, *ApJ*, 416, 415
- Hibbard, J. E. & van Gorkom, J. H. 1996, *AJ*, 111, 655
- Hjorth, J. & Madsen, J. 1991, *MNRAS*, 253, 703
- Hodapp, K.-W., Hora, J. L., Hall, D. N. B., Cowie, L. L., Metzger, M., Irwin, E., Vural, K., Kozłowski, L. J., Cabelli, S. A., Chen, C. Y., Cooper, D. E., Bostrup, G. L., Bailey, R. B., & Kleinhans, W. E. 1996, *New Astronomy*, 1, 177
- Hunt, L. K., Mannucci, F., Testi, L., Migliorini, S., Stanga, R. M., Baffa, C., Lisi, F., & Vanzi, L. 1998, *AJ*, 115, 2594
- James, P., Bate, C., Wells, M., Wright, G., & Doyon, R. 1999, *MNRAS*, 309, 585
- Jorgensen, I., Franx, M., & Kjaergaard, P. 1996, *MNRAS*, 280, 167
- Joseph, R. D. & Wright, G. S. 1985, *MNRAS*, 214, 87
- Kormendy, J. 1977, *ApJ*, 218, 333
- . 1989, *ApJ*, 342, L63
- Kormendy, J. & Sanders, D. B. 1992, *ApJ*, 390, L53

- Lake, G. & Dressler, A. 1986, *ApJ*, 310, 605
- Lynden-Bell, D. 1967, *MNRAS*, 136, 101
- Möllenhoff, C. & Heidt, J. 2001, *A&A*, 368, 16
- Mao, S. & Mo, H. J. 1998, *MNRAS*, 296, 847
- Massey, P. & Gronwall, C. 1990, *ApJ*, 358, 344
- McLean, I. S., Becklin, E. E., Bendiksen, O., Brims, G., Canfield, J., Figer, D. F., Graham, J. R., Hare, J., Lacayanga, F., Larkin, J. E., Larson, S. B., Levenson, N., Magnone, N., Teplitz, H., & Wong, W. 1998, in *Proc. SPIE Vol. 3354*, p. 566-578, *Infrared Astronomical Instrumentation*, Albert M. Fowler; Ed., 566–578
- Michard, R. & Prugniel, P. 2004, *A&A*, 423, 833
- Mihos, J. C. & Hernquist, L. 1994, *ApJ*, 437, L47
- Mobasher, B., Guzman, R., Aragon-Salamanca, A., & Zepf, S. 1999, *MNRAS*, 304, 225
- Mouhcine, M. & Lançon, A. 2002, *A&A*, 393, 149
- . 2003, *A&A*, 402, 425
- Nilson, P. 1973, *Uppsala general catalogue of galaxies (Acta Universitatis Upsaliensis. Nova Acta Regiae Societatis Scientiarum Upsaliensis - Uppsala Astronomiska Observatoriums Annaler, Uppsala: Astronomiska Observatorium, 1973)*
- Oliva, E., Origlia, L., Kotilainen, J. K., & Moorwood, A. F. M. 1995, *A&A*, 301, 55
- Oliva, E., Origlia, L., Maiolino, R., & Moorwood, A. F. M. 1999, *A&A*, 350, 9
- Origlia, L., Moorwood, A. F. M., & Oliva, E. 1993, *A&A*, 280, 536
- Pahre, M. A. 1999, *ApJS*, 124, 127
- Pahre, M. A., Djorgovski, S. G., & de Carvalho, R. R. 1998, *AJ*, 116, 1591
- Peletier, R. F. & Balcells, M. 1997, *New Astronomy*, 1, 349
- Peletier, R. F., Valentijn, E. A., Moorwood, A. F. M., & Freudling, W. 1994, *A&AS*, 108, 621
- Persson, S. E., Murphy, D. C., Krzeminski, W., Roth, M., & Rieke, M. J. 1998, *AJ*, 116, 2475
- Press, W. H., Teukolsky, S. A., Vetterling, W. T., & Flannery, B. P. 1992, *Numerical recipes in FORTRAN. The art of scientific computing* (Cambridge: University Press, 1992, 2nd ed.)
- Prugniel, P. & Simien, F. 1996, *A&A*, 309, 749

- Rix, H. & White, S. D. M. 1992, MNRAS, 254, 389
- Rothberg, B. & Joseph, R. D. 2004, AJ, 128, 2098
- Sanders, D. B. & Mirabel, I. F. 1996, ARA&A, 34, 749
- Sargent, A. & Scoville, N. 1991, ApJ, 366, L1
- Sargent, W. L. W., Young, P. J., Lynds, C. R., Boksenberg, A., Shortridge, K., & Hartwick, F. D. A. 1978, ApJ, 221, 731
- Schweizer, F. 1982, ApJ, 252, 455
- Schweizer, F. 1987, in *Nearly Normal Galaxies. From the Planck Time to the Present*, p. 18
- . 1996, AJ, 111, 109
- Scoville, N. Z., Sargent, A. I., Sanders, D. B., & Soifer, B. T. 1991, ApJ, 366, L5
- Sheinis, A. I., Bolte, M., Epps, H. W., Kibrick, R. I., Miller, J. S., Radovan, M. V., Bigelow, B. C., & Sutin, B. M. 2002, PASP, 114, 851
- Shier, L. M. & Fischer, J. 1998, ApJ, 497, 163
- Shier, L. M., Rieke, M. J., & Rieke, G. H. 1994, ApJ, 433, L9
- . 1996, ApJ, 470, 222
- Silge, J. D. & Gebhardt, K. 2003, AJ, 125, 2809
- Terlevich, R., Davies, R. L., Faber, S. M., & Burstein, D. 1981, MNRAS, 196, 381
- Tokunaga, A. T., Simons, D. A., & Vacca, W. D. 2002, PASP, 114, 180
- Tonry, J. & Davis, M. 1979, AJ, 84, 1511
- Tonry, J. L. & Davis, M. 1981, ApJ, 246, 680
- Toomre, A. 1977, in *Evolution of Galaxies and Stellar Populations*, p. 401
- van Albada, T. S. 1982, MNRAS, 201, 939
- van der Marel, R. P. & Franx, M. 1993, ApJ, 407, 525
- Vorontsov-Velyaminov, B. 1959, in *Atlas and catalog of interacting galaxies*
- Wainscoat, R. J. & Cowie, L. L. 1992, AJ, 103, 332
- Wallace, L. & Hinkle, K. 1996, ApJS, 107, 312

Whitmore, B. C., Schechter, P. L., & Kirshner, R. P. 1979, *ApJ*, 234, 68

Worthey, G., Faber, S. M., Gonzalez, J. J., & Burstein, D. 1994, *ApJS*, 94, 687

Zepf, S. E. & Silk, J. 1996, *ApJ*, 466, 114